UNIVERSITY OF CAPE TOWN
IYUNIVESITHI YASEKAPA • UNIVERSITEIT VAN KAAPSTAD

DEPARTMENT OF CIVIL ENGINEERING

THESIS

Computational Inverse Analysis of Prestressed Concrete Structures

---

Author:

Dezire Mikael ETIENNE

Supervisor:

Dr. Sebastian SKATULLA

A thesis submitted in partial fulfilment of the requirements for the degree of Bachelor in Science in Engineering in the Department of Civil Engineering

November, 2015

Plagiarism Declaration

1. I know that plagiarism is wrong. Plagiarism is to use another's work and to pretend that it is one's own.

2. I have used the Harvard Convention for citation and referencing. Each significant contribution to and quotation in this report from the work or works of other people has been attributed and has been cited and referenced.

3. This thesis is my own work

4. I have not allowed and will not allow anyone to copy my work with the intention of passing it as his or her own work.

Name	**Student No.**	**Date**	**Signed**
Dezire Mikael Etienne	DZRETI001	17/11/2015	

Abstract

Prestressed concrete has gain popularity in the civil engineering industry and found its use in structures such as bridges, nuclear power vessels, monumental towers etc. Conventional approach in designing and analyzing prestressed concrete structures consists of using experimental methods to get an actual real life response of the structure. This method, although accurate, is extremely time consuming and hence inefficient in real life work industry. This limitation can be compensated with the use of computational software where the Finite Element Method is employed. The latter alternative reveals to be much more accurate and knows no bound on the level of complexities of the structure for the analysis (Varghese and Valsson, 2012).

Considering the non-linear stress-strain relationship of concrete when subjected to strain of high order magnitude, non-linear elastic constitutive laws, already part of the framework of SEKSA, were chosen and calibrated for the study. SESKA is a structural analysis software developed by Dr. Sebastian Skatulla. The two material laws used for the process were; Neo Hookean hyperelastic material and hypoelastic material. Furthermore, upon the calibration of the required constitutive material law, implementation of an additive anisotropic material model was done by Dr. Sebastian Skatulla in an attempt to model for reinforced concrete. In the case of the modelling of the composite material of concrete with prestressing steel tendon embedded into it, the additive anisotropic material law was further developed into a prestressed body force which would represent the action of prestressing forces acting on the surface of the concrete in the anchorage area.

In computational analysis, a conventional forward method is usually used, whereby the analysis follows the construction sequence of the prestressed concrete. Although the method presents some advantages, it is limited in terms of achieving a desired deformed configuration in the final stage of the constructions sequence. This study proposes an alternative to the problem, where an inverse analysis method is introduced. The method can predict the undeformed stress-free configuration of the prestressed structures from the final known deformed configuration of the structure. Therefore, in this study, a methodology on the use of the inverse analysis method in the computational analysis of prestressed concrete is proposed, and its validation was done based on the results obtained. The method was tested on complex civil engineering megastructure to show its relevance on the area of study. For instance, a precast member from the famous Vasco da Gama Bridge was ultimately used in the computational analysis.

Acknowledgements

The author would like to acknowledge and thank the following persons who contributed in one way or another towards the completion of this document:

My supervisor, Dr. Sebastian Skatulla, for his patience in explaining advanced concepts in the area of continuum mechanics, without which I would not be able to understand the core concept of this study. Additionally, I would also thank Dr. Skatulla for his devotion in spending countless hours in the implementation of new material model type in SESKA and for his support in throughout this study.

The ICTS High Performance Computing team for allowing me to use their resources in the computational analysis of the prestressed structures in the study.

To the Ministry of Education and Human Resources, Tertiary Education and Scientific Research of the Republic of Mauritius for providing me with a 4 year scholarship under the Laureate Schemes (Rodrigues open scholarship), relieving my parents of financial pressure.

My two colleagues, Emmanuel Omatuku and Simeon Solomons, who helped me to get familiar with the software SESKA.

Finally I would like to extend many thanks to my parents, girlfriend Kate and all other friends who have supported and guided me.

Table of Contents

List of Figures

List of Tables

Abbreviations

This is the list of abbreviations that has not been defined in the text document.

ASTM	American Society for Testing and Materials
BS	British Standards
SANS	South African National Standard
SABS	South African Bureau of Standards
UDL	Uniform Distributed Load

1. Introduction

1.1 Background to study

Since its inception, prestressed concrete has evolved and established itself as a major structural material. From bridges to nuclear power vessels, from building serving every use to monumental towers, prestressed concrete has various structural application nowadays. A similar trend is expected in the design of pre-stressed concrete, where new and innovative ways in designing such, are used.

Conventional approach in designing and analyzing pre-stressed members consists of using experimental methods to get actual and accurate real life response of these structures. While this method gave accurate results, it is extremely time consuming and use of materials in the experiments reveal to be quite costly. The use of computational program where the principle of Finite Element is applied reveals to be much faster and cost effective (Varghese and Valsson, 2012).

1.2 Problem statement

In the computational simulation of the prestressed structures, a forward analysis method is usually used whereby the final stress in the concrete can be calculated after being subjected to different stress conditions. There will be different stress condition during the lifetime of the structure, starting with the initial prestressing force applied onto the concrete structure, to the different loading condition in which the structure is subjected during construction phase, finally to the service load. In the simulation, it is important to consider all the factors in chronological order to get a real time simulation of the structure. However, despite the convenience of the forward analysis in reflecting the real construction sequence, it has some limitation in achieving a desired state of the final structure per the design drawing (Tan, Yu & Zhang, 2012; Grabow, 2004).

One way to tackle this limitation is to perform a so-called inverse design analysis or "backward analysis". This will enable to calculate the stress-free configuration of the prestressed structure taking the state of the final structure as stipulated on the design drawing as a starting point and working backward to the initial reference state.

1.3 Aim of research

This study aims to calibrate material laws, which is already part of the structural analysis software SESKA, based on the elasticity theory in order to make the computational analysis of prestressed concrete structures possible. The constitutive laws concerned in the study should be able to model for concrete, reinforcing steel and prestressing steel.

Following the calibration of the constitutive laws, the study also aims to use adequate material model, such as additive anisotropic material type, in the modelling of reinforced concrete and concrete containing prestressed steel tendons.

Ultimately, the study aims to validate the use of the inverse analysis method as an alternate and improved method in the computational analysis of prestressed concrete.

1.4 Objectives

The objectives of this research are:

1. Familiarization with in-house meshfree simulation software SESKA;
2. Calibration of the constitutive material law based on elastic theory required for computational analysis;
3. Creation of simple prestressed concrete structures using the commercial pre-processing software GiD;
4. Executing computational analysis of models using the constitutive material laws;
5. Executing computational analysis on prestressed structure model when the unstressed configuration is known employing forward analysis;
6. Executing computational analysis on prestressed structure model when the unstressed configuration is not known employing inverse design analysis; and
7. Comparing both results of forward and inverse analysis.

1.5 Scope and limitations

With the recent research done in the civil engineering industry, the use of plasticity constitutive material law in concrete modelling is becoming more and more popular. Certain advantages associated with the plasticity model is that it can account for creeps and shrinkage which gives more realistic results. Although those advances have been made in the concrete modelling industry, this study will make use of constitutive law based on the elasticity theory, which is the simplest form of modelling that can be done. The reason for not giving much focus on using the complex plasticity model is that the study rather focusses on validating the use of the inverse analysis in the computational analysis of prestressed concrete structures. Therefore, the study will have some limitations in terms of modelling for creep, shrinkage, prestress losses and other factors that can usually be modelled with the plasticity theory.

Furthermore, this study does not cover the full design of prestressed of concrete where reinforcement detailing specification are usually given. It rather focusses on the understanding the implication of using the inverse analysis to achieve a final deformed shape.

1.6 Expected results of investigation

The following are the expected results of the research project:

1.6.1 Calibrating of constitutive law

It is expected that a constitutive material law based on the elasticity theory will replicate accurately the non-linear stress-strain behavior of concrete upon its calibration. Additionally, it is expected that a so-called additive anisotropy material type, which currently is not part of the framework of SESKA, is going to be implemented by Dr. Skatulla. The additive anisotropy will essentially model for reinforced concrete and concrete containing embedded prestressing steel tendon.

1.6.2 Validation of forward and inverse analysis

It is expected that the software SESKA is able to accurately predict the stress-strain behavior of prestressed concrete under the action of prestressing force and imposed loading using the conventional forward analysis method. Furthermore, the ultimate outcome of the research project is to make use of the inverse analysis method in the analysis of prestressed concrete structures. The level of discrepancy between the two methods is expected to be conclusive in the validation of the proposed inverse method.

1.7 Layout of this document

The following is a breakdown on how the research project was laid out.

Chapter one provides an introduction to the topic where a background to the research project is explained. The objectives and aim of research were also addressed. Furthermore, the scope and limitation of the thesis gives the reader a clear idea what and what not to expect from the research project.

Chapter two gives a review of the available literature on prestressed concrete. It outlines the background theory that is going to be relevant in this research project. Furthermore, the chapter also contains the design approach for prestressed concrete which contains relevant information for the forward analysis method.

Chapter three gives a background on computational mechanics theory that is necessary to understand the mechanics behind the constitutive material laws used in this study. Furthermore, the chapter gives background on the path-following method that is implemented in the in-house modelling software SESKA.

Chapter four gives a comprehensive approach to the computational analysis of prestressed concrete using the conventional forward analysis as well as the inverse analysis. The chapter also contains the calibration of the constitutive laws in order to reflect the stress-strain behavior of concrete, reinforcing steel and prestressing steel.

Chapter five is concerned with the use of proposed approach based on both the inverse and forward analysis in analyzing a portion of a bridge megastructure. By choosing a massive structure with high level of complexities in its geometry, the limits of the inverse analysis is tested.

Chapter six contains the conclusions and recommendations that were made based on the investigation performed in this study.

2. Literature review

This chapter gives a detailed literature review on the topic of prestressed concrete. It contains the underlying fundamental of prestressed concrete that is essential to understand the topic of the study. It also covers the design approach which is used in prestressed concrete design to obtain a safe structure.

2.1 Prestressed concrete

Reinforced concrete is the most widely used structural material of the 20th century (Gilbert & Mickleborough, 1990). Plain concrete has strong compressive strength but low tensile strength, hence to compensate for the latter, steel bars are usually used in conjunction with concrete in structural members.

Prestressed concrete is a particular form of reinforced concrete whereby it involves application of a normal compressive stress on the concrete member to reduce the internal tensile stresses induced by external loading. The compressive stress is achieved by using highly tensioned steel reinforcement (wire, strand, or bar) reacting on the concrete. In doing such, the method helps in eliminating crack formation within the concrete tensile zone and hence creating a crack-free material during service (Gilbert & Mickleborough, 1990; Naaman, 1982).

There is a whole area of reinforcing range between fully reinforced concrete to fully prestressed concrete called partially prestressed concrete (Naaman, 1982).

2.2 Methods of prestressing

The main methods of prestressing can be classified into two major groups; namely pre-tensioning and post-tensioning. The major difference between the two methods is the timing of the tensioning operation; the tensioning may occur before or after the concrete is cast (Gilbert & Mickleborough, 1990).

2.2.1 Pre-tensioning

In pre-tensioning method, pre-tensioning tendons, usually wires/strands, are stretched to a desired tension and anchored to fix bullheads. The concrete is then poured around the tendons, and upon hardening the tensioned tendons are released. Upon release, the steel tendon is bonded to the concrete as the concrete resist the shortening of the steel tendon. In the process, the concrete member is compressed (Gilbert & Mickleborough, 1990; Naaman, 1982). Figure 2-1 gives an overview of the procedures of pre-tensioning.

Owing to its long line mass production technique which can permit casting multiple units of prestressed concrete, pre-tensioning method is extremely convenient in the production of precast elements. Moreover, precast pre-tensioned concrete can be made into standardized cross sections depending on their application. For instance, pre-tensioned concrete used in bridge construction are usually made up of girders unit as shown in Figure 2-2 (Gilbert & Mickleborough, 1990; Naaman, 1982).

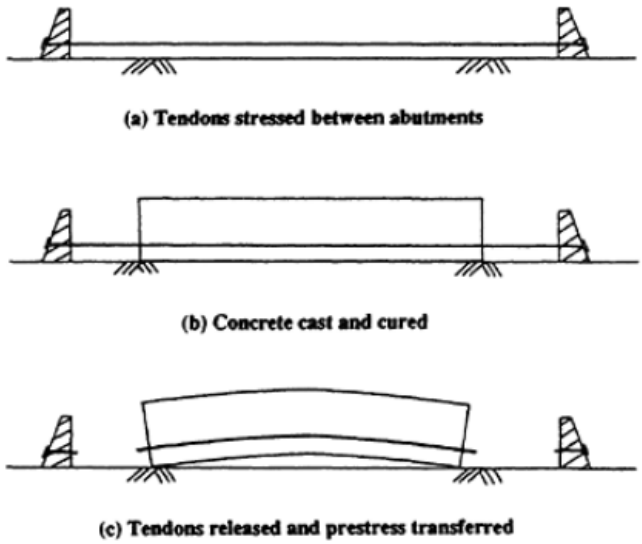

Figure 2-1: Pretensioning process (Gilbert & Mickleborough, 1990)

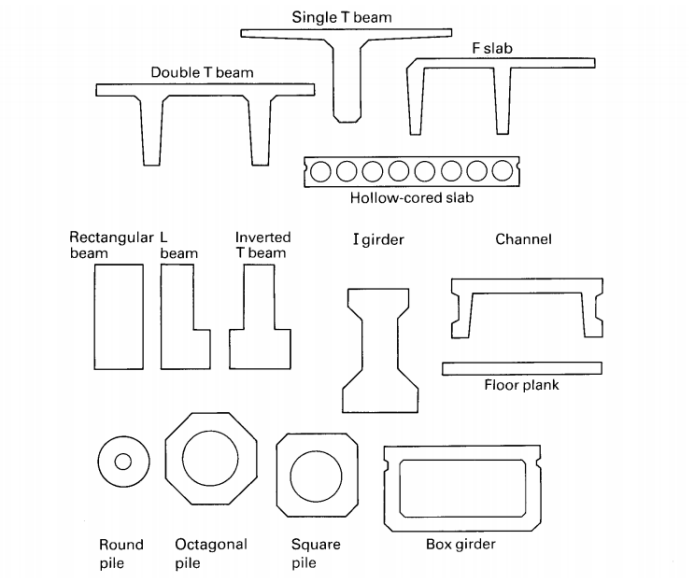

Figure 2-2: Typical cross section of precast pre-tensioned concrete (Gilbert & Mickleborough, 1990)

2.2.2 Post-tensioning

In post-tensioning, concrete is cast around hollow duct(s) which can either have a straight profile or a parabolic one depending on the designer. Once the concrete has cured for a number of required days per standards used, the steel tendon is introduced in the ducts, and stretched to a certain tension stress and then anchored at both ends. Upon anchorage, the shortening steel tendon will introduce a normal compressive stress on the concrete structure as well as a transverse force depending whether the tendon was made into a parabolic profile (Gilbert & Mickleborough, 1990).

Grouting material is usually introduced under pressure in the ducts. This will allow the steel tendon to bond with the concrete which is more efficient in controlling cracks and providing ultimate strength. However, in some countries, for economical reason, grease is introduced in the ducts instead of concrete grouting material. In this way, the tendon remain permanently unbonded (Gilbert & Mickleborough, 1990; Naaman, 1982).

Due to its practicability compared to pre-tensioning, post-tensioning method is done in situ on site rather than in industry. The light and portable hydraulic jacks makes post-tensioning an easy task on site. Figure 2-3 shows the typical procedure for post-tensioning. Prestressing tendons in post-tensioning is usually used in conjunction with reinforced concrete, hence making the structure partially prestressed.

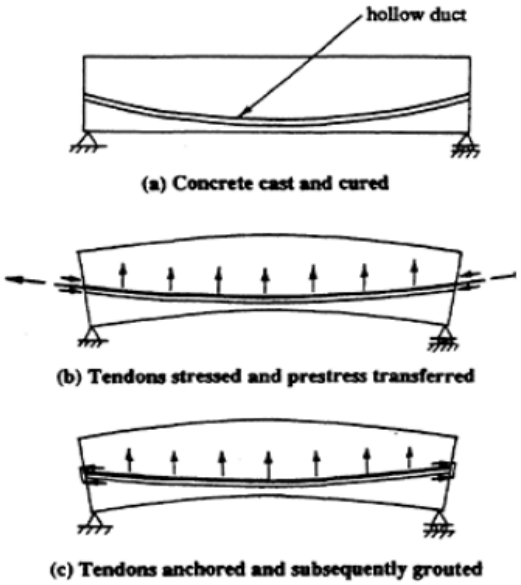

Figure 2-3: Post-tensioning process (Gilbert & Mickleborough, 1990)

2.3 Prestressed concrete materials

According to Burgoyne (2005), the effective use of prestressed concrete relies on an appropriate combination of structural analysis techniques with the knowledge of the material behavior. Hence, this chapter focus mainly of the material properties of the prestressed concrete and their behavior under loading.

Prestressed concrete is made up of two main materials namely concrete and high-strength steel. Ordinary steel is widely used in partially prestressed structure whereby there is a combination of reinforced concrete and prestressing tendon (Naaman, 1982).

2.3.1 Reinforcing steel bars

Reinforcing steel is generally used in prestressed concrete structures as shear reinforcement or additional reinforcement in region susceptible to high tensile stress and large deformation. It finds its main use in partial prestressed concrete where it provides structural resistance to an extent as prestressing steel. Moreover, in seismic design, reinforcing steel is also placed in both tensile and compressive zone of the structure. The characteristic strength of reinforcing steels bars according to the British Standards is shown in Table 2-1. Moreover, the stress-strain relationship of a reinforcing steel bar is shown in Figure 2-4.

Table 2-1: Reinforcement strength (BS 5400-4-1990)

Designation	Nominal sizes	Characteristic strength, f_y
	mm	N/mm^2
Grade 250 (BS 4449)	8, 10, 12, and 16	250
Grade 460 (BS 4449)	All sizes	460
Cold reduced steel wire (BS 4482)	Up to and including 12	485

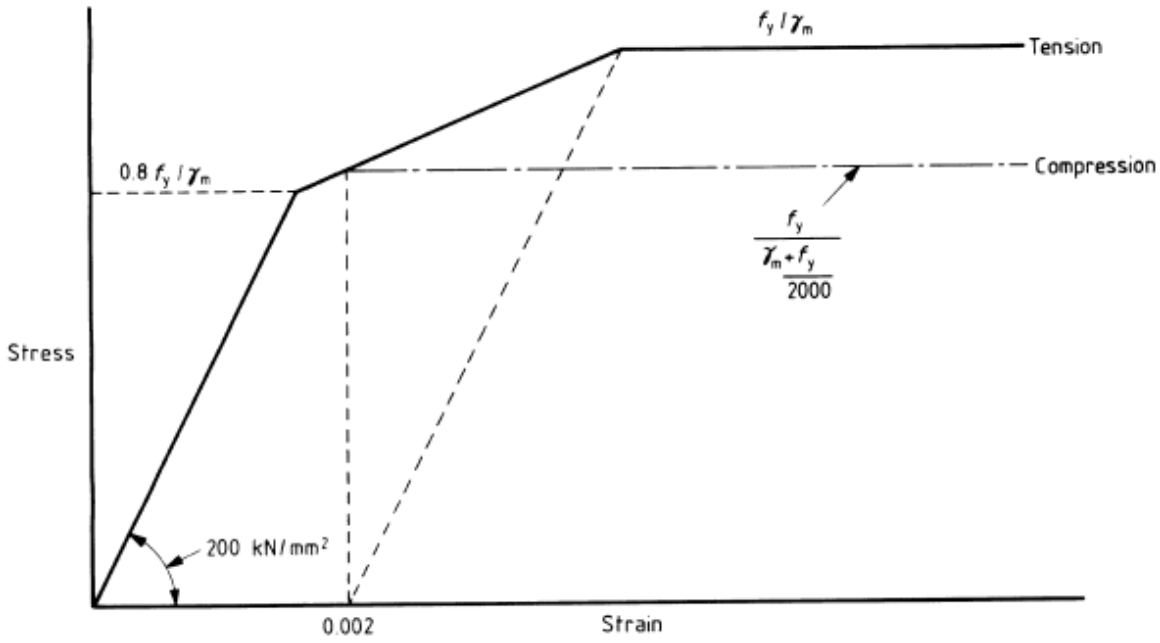

Figure 2-4: Short term stress-strain curve for reinforcement (BS5400-4-1990)

where f_y is the characteristics strength of reinforcement, γ_m is the partial safety factor for strength.

2.3.2 Prestressing steel tendons

To minimize prestress losses due to the prestressing process, it is important that the prestressing steel tendon enables long elongations. The prestressed losses in concrete members usually reach values up to 414 MPa, which is approximately equivalent to the typical yield strength of ordinary reinforcing steel. Hence for effective stress transfer, steel of higher tensile strength than ordinary reinforcing steel is needed for the process of prestressing (Naaman, 1982). Typical tensile strength of prestressing tendons used in the United States are illustrated in Table 2-2. When subjected to uniaxial tension during prestressing operation, a stress-strain curve relationship is obtained as shown in Figure 2-5

Table 2-2: Typical characteristics of prestressing bars (Naaman, 1982)

Type	ASTM grade	Nominal diameter		Nominal area†		Minimum tensile strength f_{pu}	
		in	mm	in^2	mm^2	ksi	MPa
Smooth alloyed steel bars (ASTM A722)	145	0.750	19.05	0.442	283.9	145	1000
		0.875	22.22	0.601	387.1	145	1000
		1.0	25.40	0.785	503.2	145	1000
		1.125	28.57	0.994	638.7	145	1000
		1.250	31.75	1.227	793.5	145	1000
		1.375	34.92	1.485	954.8	145	1000
	160	0.750	19.05	0.442	283.9	160	1104
		0.875	22.22	0.601	387.1	160	1104
		1.0	25.40	0.785	503.2	160	1104
		1.125	28.57	0.994	638.7	160	1104
		1.250	31.75	1.227	793.5	160	1104
		1.375	34.92	1.485	954.8	160	1104
Deformed bars‡	…	0.625	15.87	0.280	180.6	157	1083
		1.0	25.4	0.852	548.4	150	1035
		1.0	25.4	0.852	548.4	160	1104
		1.25	31.75	1.295	835.5	150	1035
		1.25	31.75	1.295	835.5	160	1104
		1.50	34.92	1.630	1051.6	150	1035

†Bar density = 490 lb/ft^3 or 7850 kg/m^3.
‡Adapted from the *PCI Handbook*.

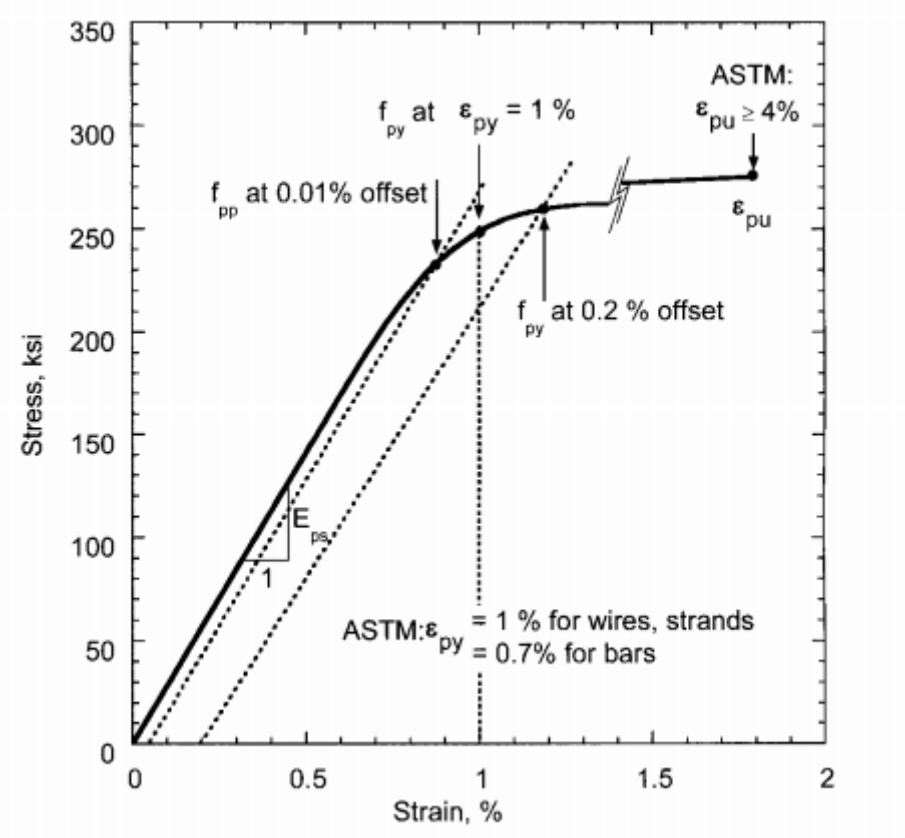

Figure 2-5: Stress-strain relationship of prestressing steel tendon under uniaxial load (Naaman, 1982)

The stress- strain curve can be represented into 3 portions;

1. An initial linear elastic portion up to proportional limit;
2. A non-linear portion with gradually decreasing slope; and
3. A final almost linear strain-hardening portion with a small positive slope leading to failure.

According to Naaman (1982), yielding of prestressing steels is usually not well defined, hence their yield are determined according to strain criterion. Specification from ASTM states that the yield stress of prestressing wires and strands should correspond to a total strain of one percent. Moreover, the recommended total strain for prestressing bars is 0.7 percent.

2.3.3 Concrete

2.3.3.1 Composition of concrete

Concrete is made up of a mixture of cement, aggregates and water. Depending on its application, it may also contain chemical admixtures. In a concrete mixture, the proportion of the material is not definite and may vary depending on the designers' specifications. A typical mix used for prestressed concrete by weight can be; 44% coarse aggregate, 31% fine aggregate, 18% cement and 7% water (Gilbert & Mickleborough, 1990).

The minimum water-to-cement ratio required for complete hydration of cement is about 0.25. However, larger proportion of water is needed to produce a workable concrete mix. A typical water-to-cement ratio for prestressed concrete is about 0.4. Although water increase the workability of concrete mixture, it is recommended to use the minimum water possible as the water not used in hydration causes voids in the cement paste than reduce the strength and increase the permeability of concrete (Gilbert & Mickleborough, 1990). This encourages crack propagation hence making the structure less safe under service load.

In the past years, low water-to-cement ratio has been made more workable by adding chemical admixtures in the concrete mix. In doing so, this helps to attain a higher concrete strength with low permeability (Gilbert & Mickleborough, 1990).

2.3.3.2 Strength of concrete

Prestressed concrete are usually subjected to relatively higher forces and load that a reinforced concrete usually experienced. Therefore, it is important to use higher strength concrete to be able to take stresses induced from the higher forces and loads.

In practice, prestressed concrete is of better quality and has higher strength than in normal reinforced concrete. A typical range of characteristic strength, f_c , of prestressed concrete is within 30-40 MPa, although in some cases concrete strength of over 100 MPa have been used successfully in North America. As the compressive strength of the concrete increases, so does the tensile strength. Therefore, the use of high strength concrete may delay the onset of cracking in a member (Gilbert & Mickleborough, 1990).

2.3.3.3 Stress-strain curve

A typical stress strain curve for concrete with different strength is shown in Figure 2-6. The concrete is subjected to uniaxial compression as it would experience in prestressing process.

The curve is comprised of 2 parts; an ascending slope up to the peak point and a descending slope. The ascending slope can be separated into a linear part and non-linear part. The linear part extend up to about 40 percent of the strength, followed by the non-linear part up the peak stress. The strength, f_c, correspond to the peak point, which is the maximum stress.

In the non-linear part of the stress-curve, the total strain is composed two parts; an elastic strain and a permanent irrecoverable strain. The irrecoverable strain is mainly due to micro cracking (Naaman, 1982).

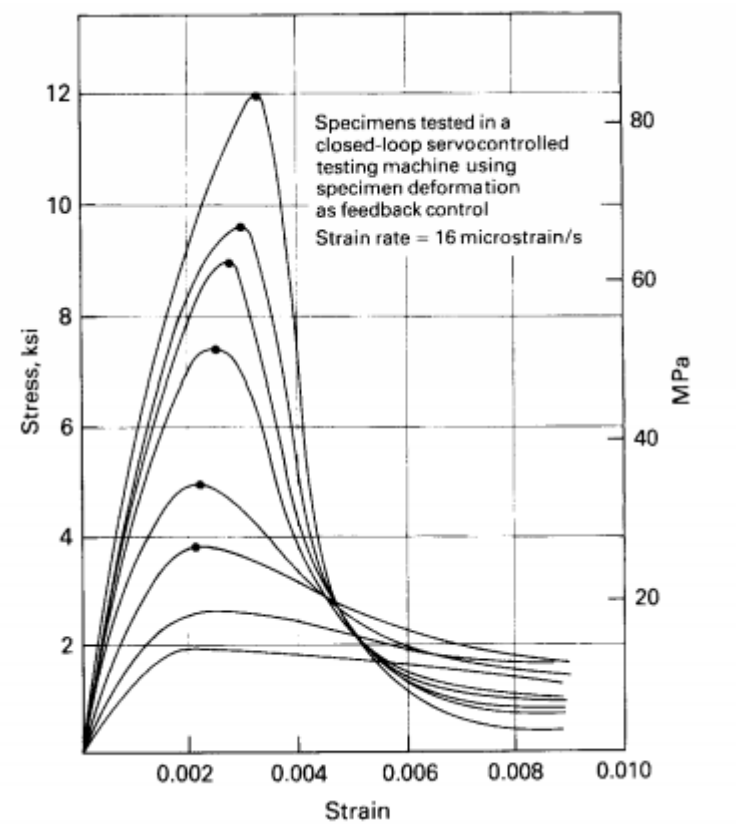

Figure 2-6: Typical stress-strain curve of concrete subjected to uniaxial compression (Naaman, 1982)

2.3.3.4 Shrinkage

As discussed previously in section 2.3.3.1, although the minimum water-to-cement required for complete hydration is about 0.25, higher proportion is usually needed to produce a workable concrete. This usually leaves excess water in the concrete matrix. The excess water that is not chemically used the hydration reaction of the cement is called the free water. Upon evaporation the loss of the free water leads to a gradual shortening of the member with time, and this is defined as shrinkage. Shortening of the member leads to prestressing steel losses in the member also referred to as shrinkage loss. Shrinkage loss is illustrated in Figure 2-7.

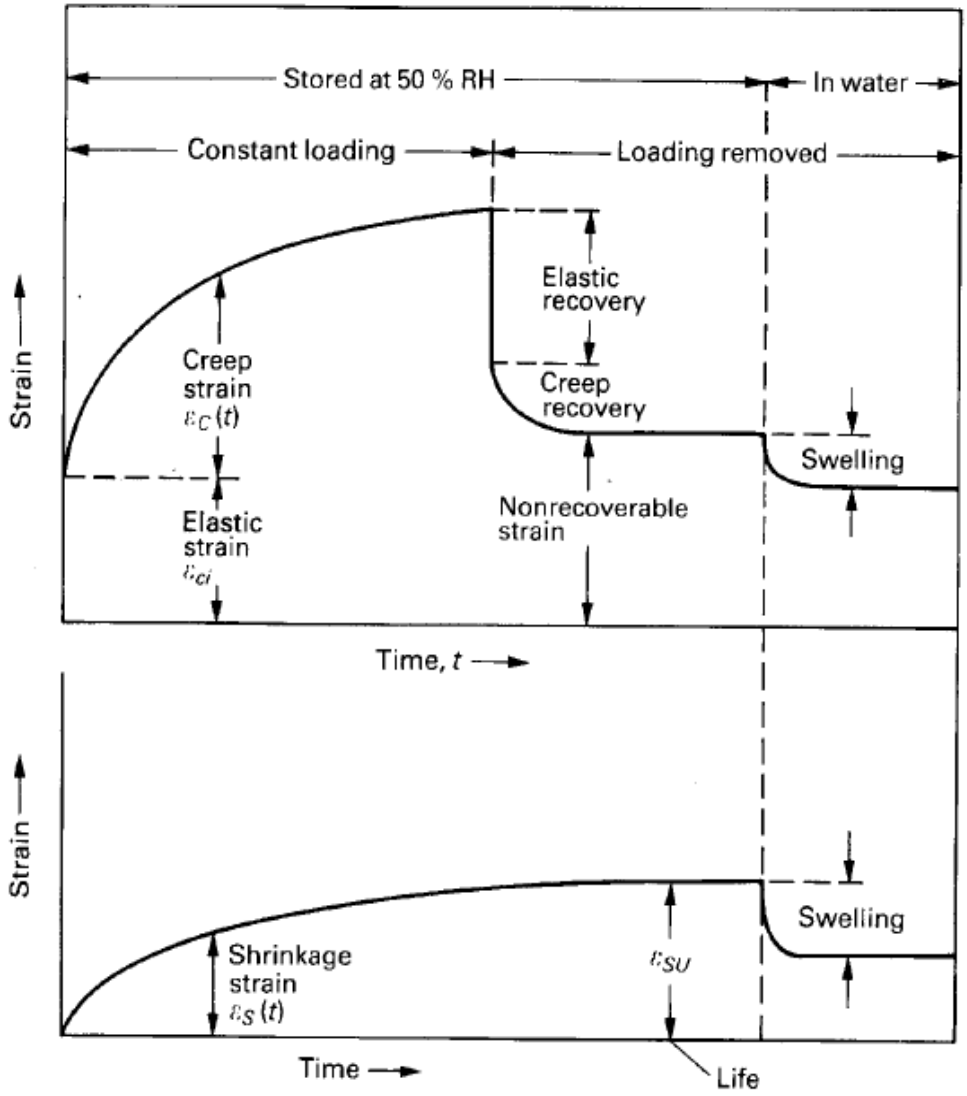

Figure 2-7: Variation over time of shrinkage and creep strain of concrete (Naaman, 1982)

Shrinkage depends on a number of factors, namely:

- Amount of free water, hence the water-to-cement ratio;
- The relative humidity of the environment;
- The ambient temperature;
- The type of aggregates used; and
- The shape of the structural member.

2.3.3.5 Creep

According to Naaman (1982), creep is a time-dependent strain in excess of elastic strain normally induced in a material subjected to a constant stress. If the load causing the stress is removed, the initial elastic strain is recovered immediately while only a part

of the creep strain is gradually recovered over time. The remaining part of the strain that has not recovered is referred to as the non-recoverable part. This is illustrated in Figure 2-7.

If the load is maintained, the creep strain tends asymptotically toward a maximum value ε_{cu} referred to as creep strain. Creep is very relevant to prestressed concrete member since the latter is always under big axial compression. This will eventually induce considerate stress losses in the steel and long-term deflection of the member (Naaman, 1982).

2.4 Stress induced in prestressed concrete

According to Lin & Burns (1981), prestressed concrete can be visualized as being subjected to two systems of forces; the internal prestress and external load. The tensile stresses induced by the external load is counteracted by the compressive stress due to the prestress force. This system of forces can be explained by a simple loading scenario as follows;

Figure 2-8 shows a plain rectangular concrete beam prestressed by a steel tendon at its centroid axis and loaded by an external load. The prestressed force F acting on a cross sectional area A of the concrete will produce a compressive stress as follows:

$$\sigma = \frac{F}{A} \qquad \textit{Equation 2-1}$$

If there is an induced external moment M due to the external loads and weight of the concrete beam, then the stress at any point across the section due to M is

$$\sigma = \frac{My}{I} \qquad \textit{Equation 2-2}$$

where y is the distance from the centroid axis and I is the moment of inertia of the section. The resultant stress is represented in Equation 2-3.

$$\sigma = \frac{My}{I} \pm \frac{F}{A} \qquad \textit{Equation 2-3}$$

When the tendon is acting at an eccentricity e with respect to the centroid axis, it creates an external hogging moment. Figure 2-9 shows a prestressed concrete section with prestress steel tendon acting at an eccentricity e from the centroid axis. The

moment is represented as Fe, and the stresses across the section due to this moment is as follows:

$$\sigma = \frac{Fey}{I} \qquad \textit{Equation 2-4}$$

Hence the expression for the total stress in the structure is given by:

$$\sigma = \frac{My}{I} \pm \frac{Fey}{I} \pm \frac{F}{A} \qquad \textit{Equation 2-5}$$

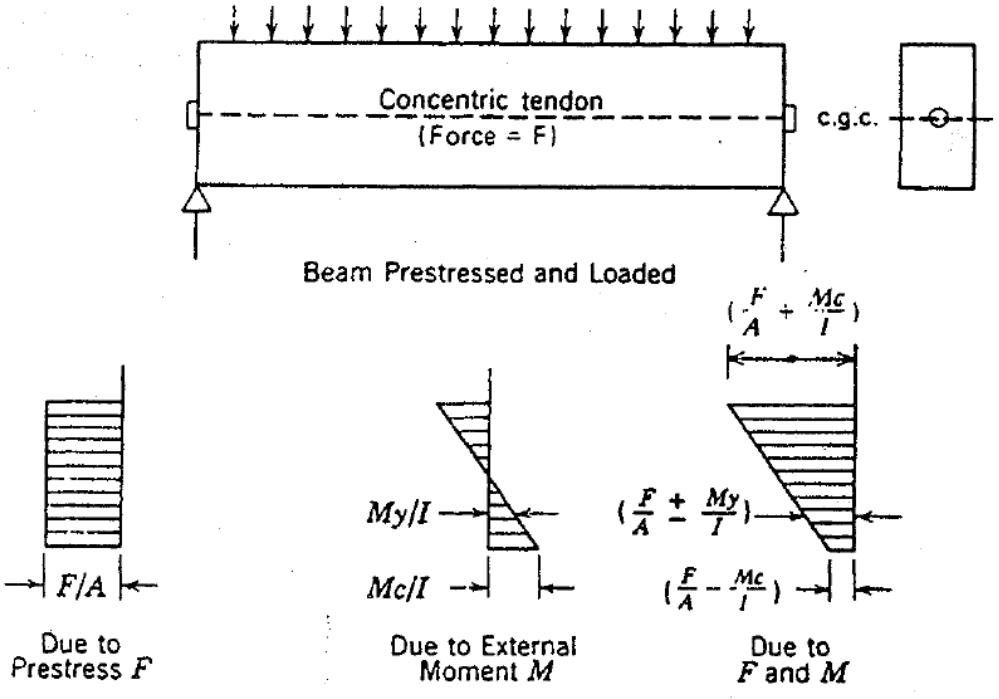

Figure 2-8: Stress distribution across a prestressed concrete with steel tendon acting at the centroid axis (Lin & Burns, 1981)

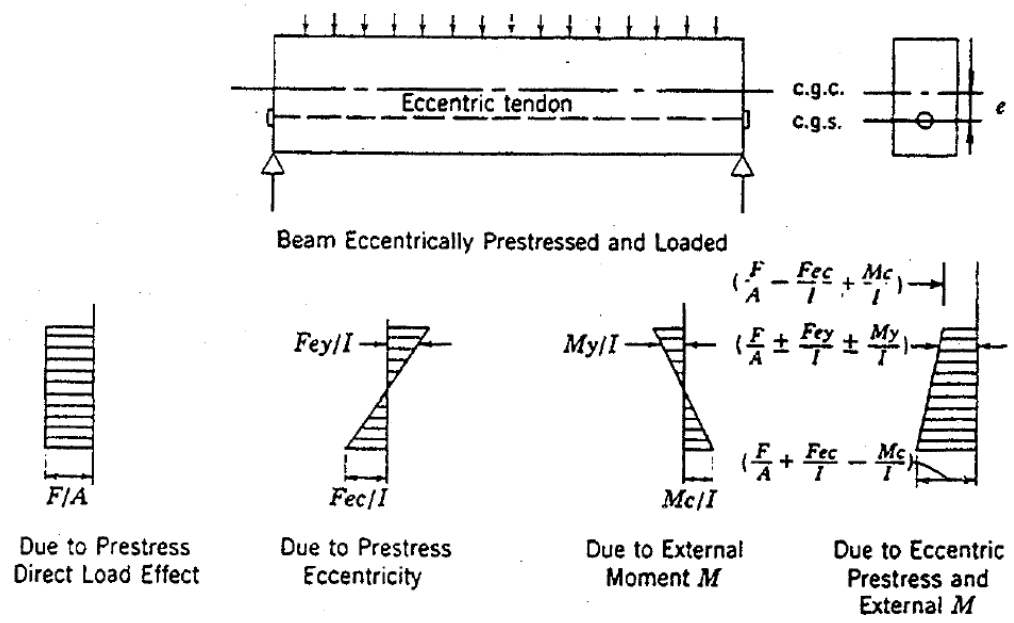

Figure 2-9: Stress distribution across a prestressed concrete with steel tendon acting at an eccentricity (Lin & Burns, 1981)

2.5 Prestress losses

Upon transfer, i.e. when the steel tendon start exerting forces on the concrete face, the steel tendon experiences losses along its length due to friction between the concrete and the tendon. Moreover, further losses occur over the long term after lock off. These are caused by elastic shortening, creep and shrinkage of the surrounding concrete and relaxation of the steel tendon (Hewson, 2003). The long term expression for prestress losses can be expressed as follows:

$$f_{pc} = f_p - l_E - l_r - l_c - l_s \qquad \textit{Equation 2-6}$$

where l_s = stress loss due to shrinkage

l_c = stress loss due to creep

l_r = stress loss due to relaxation of steel

l_E = stress loss ude to elastic shortening

f_P = initial stress in steel tendon

The initial stress at which a tendon may be stressed depend on the ultimate tensile strength (UTS) of the steel tendon. Although tendons can be stressed up to 80% UTS, some design codes specify limits on jacking force to 75% UTS, and a maximum force in the tendon after release to a maximum of 75% UTS (Hewson, 2003).

2.5.1 Friction losses and tendon losses

When prestressing bars and pretension wires or strands are placed in a straight profile, only few friction losses are usually experienced. However, when tendons are made to follow a curved profile, this causes the strands to press against the sides of the duct which induces significant friction. For instance, the losses along the length of the curved tendon is expressed in terms of θ , the friction coefficient action on the angle change in the tendon profile, and k, the wobble effect acting along the length of the tendon. The wobble effect is essentially the unitentional local misalignment of the duct, which results in the tendon getting in contact with the duct, hence causing friction (Hewson, 2003). Taking into account losses due to friction, the expression for the force, F at any point, x metres along the tendon from the anchor can be expressed as follows:

$$F = F_0 e^{-(\mu\theta + kx)} \qquad \textit{Equation 2-7}$$

where F_0 = initial applied force
θ = angle change in the tendon profile
μ = friction coefficient
k = friction coefficient due to wobble
x = distance in meters along the tendon profile from the anchorage point

Specifications for friction coefficients are usually obtained from the manufacturers litterature for the type of steel tendon being used. In cases where external tendon, bar or pre-tensioned strand are used, the friction coefficient due to wobble, $k=0$ (Hewson, 2003).

A typical force profile is shown in Figure 2-10. For tendons longer than 40 m and with large angle changes, significant large losses can occur within the ducts. One way to limit this is by using double-end stressing method, where the tendon is jacked at both ends of the beam (Hewson, 2003).

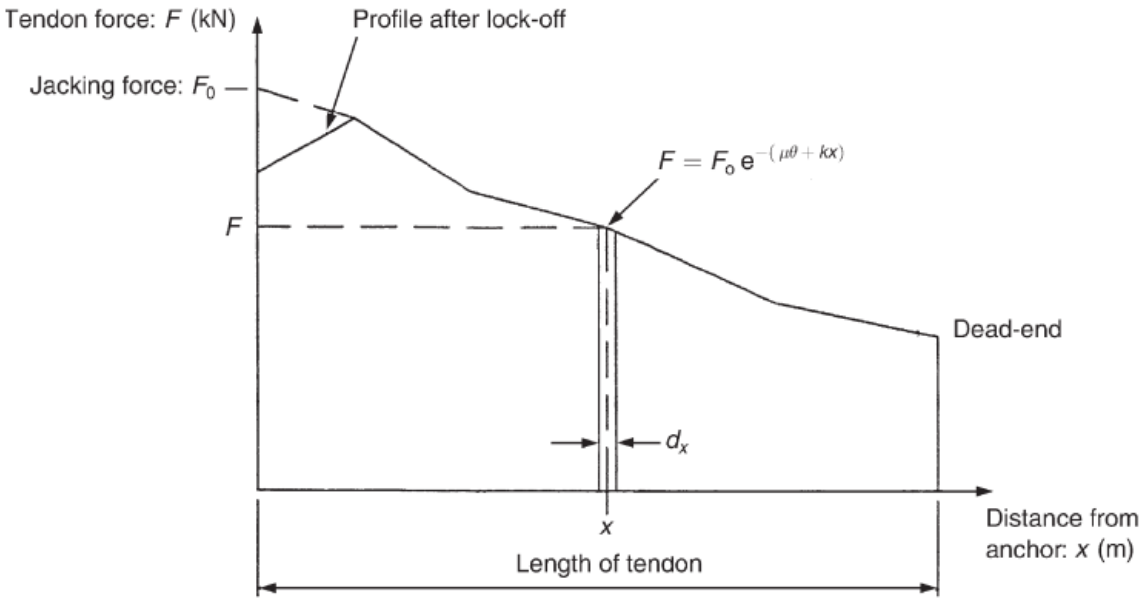

Figure 2-10: Force profile across the length of the tendon (Hewson, 2003)

2.5.2 Elastic shortening and strains

Mechanical behavior of concrete also affects the losses in the steel tendon. For instance, elastic shortening of concrete under the application of concentrated force causes stress losses in any tendons that have been previously installed (Hewson, 2003). The stress loss due to elastic shortening of concrete can be expressed as follows:

$$l_E = \sigma_c (E_t / E_c) \qquad \textit{Equation 2-8}$$

where σ_c = increase in stress in concrete adjacent to the tendon
E_t = young modulus of steel tendon
E_c = young modulus of concrete

As the concrete member deflects when subjected to imposed loading and live loads, the stress and strain level along the whole length of the concrete changes, as a consequence, changes in prestressed losses is to be expected. However, it was found that the effect is so small that it can be neglected without compromising the prestress design (Hewson, 2003).

2.5.3 Relaxation of steel tendon

After the force has been applied in the prestressing tendon to the concrete, there is a general reduction in the force in the tendon and this is referred to a relaxation. Figure 2-11 shows a graph relaxation vs initial stress in tendon. From the graph, the relaxation of the stress in the prestressing steel can be seen to be dependent on the initial stress in the steel tendon and on the material properties of the steel (Hewson, 2003).

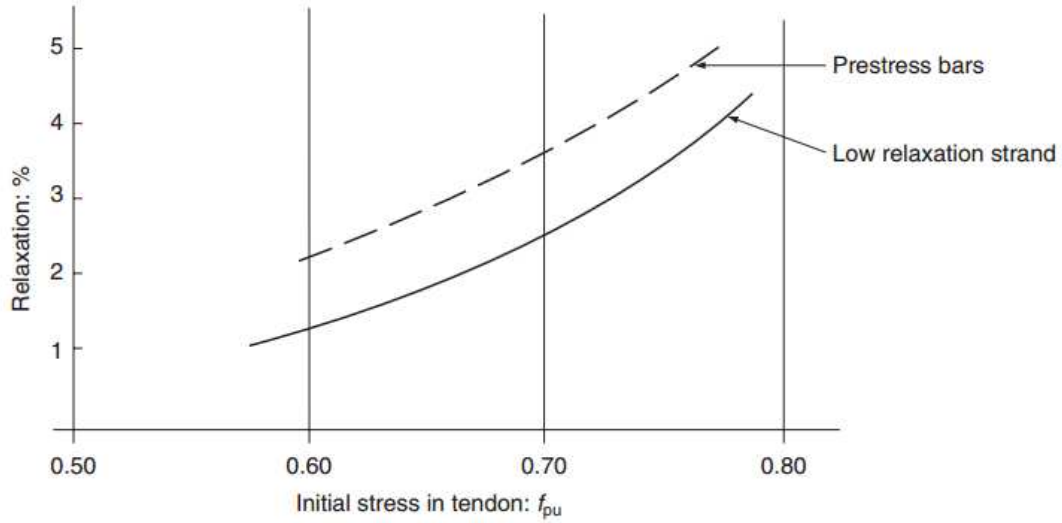

Figure 2-11: Percentage relaxation vs initial stress in tendon (Hewson, 2003)

2.5.4 Creep Losses

The effect of creep in concrete also affect the level of stress and strain in the imbedded tendons, hence affecting its prestressed losses (Hewson, 2003). The loss of stress in a tendon due to creep can be expressed by:

$$l_E = \phi\sigma_c(E_t / E_c) \qquad \textit{Equation 2-9}$$

where ϕ = creep factor

The creep factor is dependent on the concrete mix, environmental casting conditions and the maturity of concrete. For bridge design, the value of creep factors is the range of 1.6 to 2.5 (Hewson, 2003). BS 5400 also offers specification for the creep factors. For instance, Appendix C of BS 5400 provides charts where creep factor ϕ can be derived.

According to Hewson (2003), the presence of reinforcement can reduce the creep of the concrete. However, the percentage of reinforcement is usually low in prestressing members, hence the effect of reinforcement on the creep losses is usually negligible.

2.5.5 Shrinkage losses

In addition to creep, concrete shrinkage also causes the shortening of steel tendon and, therefore a reduction in stress and strain in steel tendons. The losses due to shrinkage can be expressed as follows:

$$l_s = \Delta_{cs} E_t \qquad \textit{Equation 2-10}$$

where Δ_{cs} = shrinkage strain in the concrete after the installation of the tendon.

Appendix C of BS 5400, provides guidance where shrinkage strain Δ_{cs} can be derived. Moreoever, clause 6.7.2.4 of BS5400-4-1990 gives specification of shrinkage strain based on a number of parameters such as humidity of the casting environment and ages of concrete at transfer.

2.6 Forces applied by prestress anchorages

The axial force from prestressed cable generally develop stresses of high magnitude in areas near the anchorage zone of the prestressed structure. Owing to this fact, three areas behind an anchor need to be reinforced. The mechanism of stress transfer is explained in this chapter which gives a better understanding of how the critical stresses are developed in these areas (Benaim, 2008).

2.6.1 Splitting forces behind anchorages

Upon release, the anchor has a tendency to be driven into the concrete member by the mere force in the tendon and this causes splitting forces in the cross section along the length of the structure. For instance, the splitting force mechanism is shown Figure 2-12. The change in direction of the axial line force creates transverse stresses; compression if the lines are concave towards the center line, and tensile when convex. Therefore, splitting and or bursting reinforcement are required to resist these transverse tensile stresses. The reinforcement usually consist of spirals or a series of mats (Benaim, 2008).

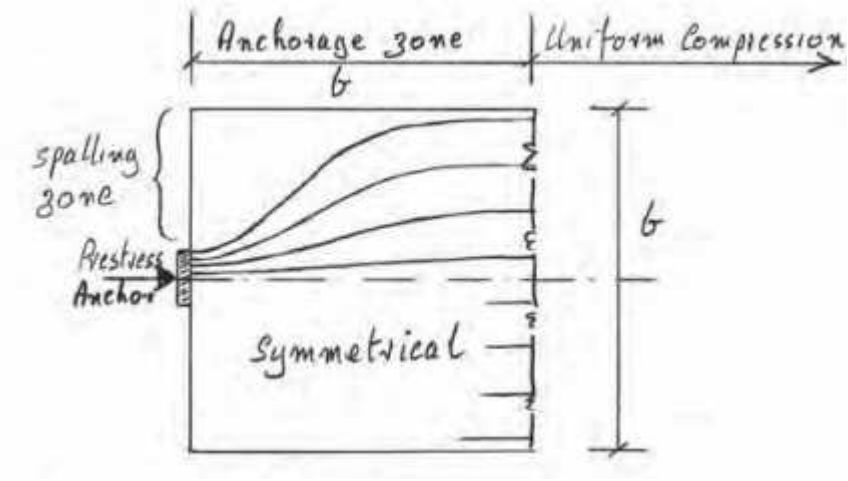

Figure 2-12: Stress mechanism behind a prestress anchor (Benaim, 2008)

2.6.2 Spalling

The tensile zone adjacent to the anchor on the end face of the member is referred to as the spalling zone. As discussed above in section 2.6.1, the compressive force of the anchor gets carried along the stress trajectories as in Figure 2-12. The concrete within these trajectories tend to shorten under the effect of the compressive stresses. However, the concrete area that are found outside the trajectories path is not subjected to the same compression. As a result, strain discontinuity is developed between the two zones of compression and non-compression creating shearing and tensile stresses in the concrete adjacent to the anchor, i.e. in the spalling zone. The spalling zone is illustrated in Figure 2-12. Up to a certain value, the tension can cause the concrete to break away exposing the reinforcement and cause serious durability issue. However, the forces involved in the spalling effect are small and therefore, the area only needs to be reinforced with small-diameter bars, typically not larger than 10 mm. The reinforcement bar can be bent into tight radii and fixed into the corners of the concrete member (Benaim, 2008).

2.6.3 Dispersion of the prestress

When prestressed forces propagate in a slab or bridge deck, zone of tensile stresses is created. The effect is illustrated in Figure 2-13 which shows a top view of a slab prestressed by two steel tendons near its edges. The tensile stress induced in the slab can be explained by visualizing the slab being cut down across its axis as shown in Figure 2-14. It can be seen that the compressive force from the anchorage area on the edge of each side of the slab will cause the slab to crack in the middle, splitting it even more. Therefore, it is clear that a tie force in the form of reinforcement is required along the axis of the deck to limit this splitting effect (Benaim, 2008).

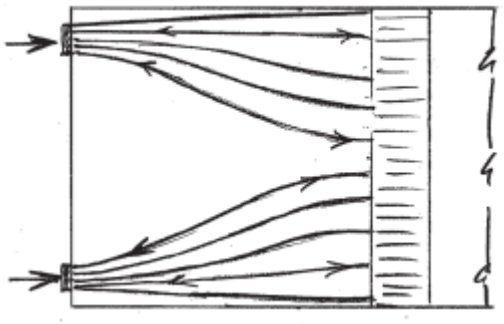

Figure 2-13: Force trajectories (Benaim, 2008)

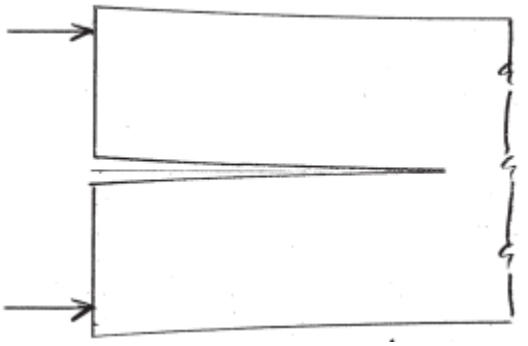

Figure 2-14: Split slab analogy (Benaim, 2008)

2.7 Design approach

The basic fundamentals of prestressed concrete were discussed in the previous sections, where understanding of how prestressed concrete works under the action of forces can be obtained. As an extension to the previous sections, this chapter highlights the design procedures based on the limit state approach.

2.7.1 Limit states

Design codes normally used in South Africa for the design of prestressed concrete structures are based on the limit states design approach (Marshall, 1995). The limit states approach offers a practical procedure to ensure that there is acceptable probability that the structure will remain fit for its intended use during its design life. Any condition at which the structure may become unfit for use is called the limit state, and the objective of a design is to ensure such limit states are not reached (Marshall, 1995). There are two types of limit states, namely the ultimate limit state (ULS) and the serviceability limit state (SLS).

2.7.1.1 Ultimate limit state

The ultimate limit state is concerned with the maximum load-carrying capacity of the structure. It can be classified into the following categories:

- Stability

  The structure must remain stable under critical load combinations. The requirement for the design is that the ultimate limit state of the structure must not be reached by rupture of any section, by overturning or by buckling.

- Robustness

  The structure must be robust in such a way that any damage in the small part of the structure will not lead to the collapse of the major part of the structure. Therefore, this criteria is important as it accounts for damage caused by the events of accidents.

2.7.1.2 Serviceability limit state

The serviceability limit state is concerned with the normal use and durability of the structure. It can be classified into the following categories:

- Deflection
  Limitation are set on the allowable deformation of the structure to ensure that neither its appearance nor performance are affected. The limitations set minimize damage that deformations can cause to other structural elements such as finishes, partitions, glazing and cladding.
- Cracking
  Crack width is controlled to ensure that the durability of the structure is not compromised.
- Vibration
  Vibration is controlled to a certain level to prevent discomfort and alarm occupants of the structure.

In the design of the limit states in prestressed concrete, the normal procedure is to design on the expected critical limit states, and then to examine the other limit states to check if they have not been reached. In the design codes of practice used in South Africa, prestressed concrete are categorized on the critical limit states which govern their design. The categories are as follows:

- Class 1 (Fully prestressed): No tensile permitted
- Class 2 (limited prestressed): Tensile stresses permitted to a certain extent where no visible cracks will develop
- Class 3 (partial prestressed): Tensile stresses permitted, with surface cracks limited to values prescribed by the codes being used.

The design of class 1 and class 2 are governed by the serviceability limit state of cracking, while the design of class 3 can be governed by the ultimate limit state or the serviceability limit state of deflection (Marshall, 1995).

2.7.2 Design for serviceability limit state

The design code of practice of South Africa sets certain limitations on the concrete flexural tensile stresses to limit the crack width of the structure. Additionally, the code also gives specifications on the maximum stresses to be respected within the concrete structure. It is believed that the limitations for the compressive stresses are set to prevent the development of excessive creep strains in the concrete and to prevent micro-cracking and spalling of the concrete in the compression zone. The concrete stress limitations specified by SABS 0100 are listed in Table 2-3 (Marshall, 1995).

Generally, in the design of prestressed concrete, the tensile stresses should be checked at a number of critical stages. Of these critical stages, the "transfer" stage where prestressing force and dead load are the only force acting on the structure and the "SLS" stage where maximum load is applied appear to be the most important stages. Hence, the structure is designed for these two stages. Table 2-3 provides specifications for these two stages (Marshall, 1995).

Table 2-3: Limiting concrete stresses in prestressed members (Robert, Year) (SABS 0100)

	Class 1 members	Class 2 members	
		Pre-tensioned	Post-tensioned
At Transfer			
1. Compression			
Triangular or near Triangular distribution of prestress	$0.45f_{ci}$	$0.45f_{ci}$	$0.45f_{ci}$
Near uniform distribution of prestress	$0.3f_{ci}$	$0.3f_{ci}$	$0.3f_{ci}$
2. Tension	$1.0MPa$	$0.45\sqrt{f_{ci}}$	$0.36\sqrt{f_{ci}}$
Serviceability limit state (SLS)			
1. Compression			
Design Load in bending	$0.33f_{cu}$ *	$0.33f_{cu}$ *	$0.33f_{cu}$ *
Design load in direct compression	$0.25f_{cu}$	$0.25f_{cu}$	$0.25f_{cu}$
2. Tension	0	$0.45\sqrt{f_{cu}}$ **	$0.36\sqrt{f_{cu}}$ **

f_{ci} = Concrete compressive strength at transfer

* Within range of support moments in continuous beams and other statically indeterminate structures this limit may be increased to $0.4f_{cu}$

** These stresses may be increased under certain conditions, as specified in SABS 0100

2.7.3 Design for ultimate limit state

Flexural design for ultimate limit state essentially consists of determining and calculating the area of concrete under compression, the effective depth of the prestressing steel and the area of steel needed to withstand required flexural strength at the ultimate limit state (Marshall, 1995).

Derived from expressions of moment and horizontal force equilibrium, the following equilibrium equations can be used to calculate the area of steel and area of concrete required to withstand a certain moment. Where Equation 2-11 shows the moment equilibrium equation while Equation 2-12 shows the force equilibrium equation.

$$M_u = A_{ps} f_{ps} z \qquad \textit{Equation 2-11}$$

$$A_{ps} f_{ps} + \alpha f_{cu} A'_c = 0 \qquad \textit{Equation 2-12}$$

where z = internal lever arm
A'_c = concrete area under compression at ultimate

The equation rearranged gives the following:

$$A_{ps} = \frac{M_u}{f_{ps} z} \qquad \textit{Equation 2-13}$$

$$A'_c = -\frac{A_{ps} f_{ps}}{\alpha f_{cu}} \qquad \textit{Equation 2-14}$$

The design process is summarized as follows:

1. Assumptions made for values for f_{ps}, z and for overall section depth h
   - For bonded tendons, f_{ps} is initially taken as the design value of f_{pu} (characteristic strength of the tendon), while for unbonded tendons , it is taken as $0.7 f_{pu}$
   - z usually ranges between 0.6h and 0.9 h, depending on the section shape; therefore it is acceptable to take $z = 0.8$h.
2. Estimate of the required area of prestressing steel A_{ps} can be obtained using Equation 2-13.
3. Consequently, the required concrete compression area A'_c can be obtained using Equation 2-14. At this stage, enough information is available to select a section or validate a section.
4. Once the preliminary values are obtained, the actual values of f_{ps} and z corresponding to the selected section can be determined. Consequently, an improved value for A_{ps} and A'_c can be calculated using Equation 2-13 and Equation 2-14 respectively. The process is repeated until a satisfactory section is obtained.
5. Finally, with all the parameters for the section obtained, the ultimate moment of resistance of the section is checked against the moment produced by the imposed loads.

2.7.3.1 Deflections

Normal practice in prestressed concrete design requires the structure to be designed on the basis of flexure either at the serviceability limit state or the ultimate limit states depending on the class of the material (Marshall, 1995). Further step is to check the

code requirements with regards to shear. Ultimately, the structure is checked for other serviceability limits states such as deflection.

The basic idea behind prestressed concrete is that the prestress force is made to induce an upward deflection which will be opposite and, ideally, equal to the downward deflection induced by external loads. For instance, in a simply supported beam, the uniform distributed load will induce a downward deflection δ_u while the prestress force will induce an upward deflection δ_p. The total deflection of the beam is therefore given by the following equation:

$$\delta_T = \delta_u + \delta_p \qquad \textit{Equation 2-15}$$

Similar to the section 2.7.2, deflections must also be checked at the critical stages of the prestressed concrete design.

At transfer stage

At transfer, upon the release of the prestressing steel tendon onto the concrete anchorage, the prestress force is acting at its maximum since long-term losses have not yet taken place. On the other hand, the external load will be acting at its minimum value since only the self weight dead load is accounted for at this stage. As a consequence, the upward deflection δ_p will normally be much larger than the downward deflection δ_u (Marshall, 1995).

At the SLS stage

In the final stage, long-term stresses have already taken place and the prestress forces will be acting at its minimum value. With the additional live load and superimposed load, the external loads will be at its maximum. Depending on the reduced value of δ_p after prestress losses, the final deflection after the application of the external dead load can be either be upward or downward. If the reduced δ_p is still larger than δ_u, the deflection will be upward and if δ_p is smaller than δ_u, the deflection will be downwards (Marshall, 1995).

Exessive deflection sometimes may be an eyesore and cause public concern on the integrity of the structure. Additionally, excessive deflection can cause damage to structural and non-structural elements. Therefore, it is important to set some limitations on the deflections of prestressed structures (Marshall, 1995). The following aspects should be considered with regards to deflection:

- Sensory acceptability: it deals with the visual acceptability (such as sagging beams and slabs, drooping cantilivers), tangible and auditory effects which arise from vibrations due to dynamic loads
- Loss of serviceability of the structure: this covers aspects which ensure that the structure will maintain its design purpose over its lifetime. This can include ponding of slab, excessive deflection of members supporting sensitive equipments ..

- Effects on non-structural elements: excessive deflections can cause damage to non-structural members such as partitions and finishes, and can also damage windows and doors.
- Effects on structural elements: excessive deflections can modify, to a certain extent the load carrying mechanism of a structural element, ultimately reducing its capacity. For instance, excessive transverse deflection can initiate stability failure of a slender column.

SABS 0100 gives the following limitations standards which can be used as guidelines:

1. Final long-term deflection should not exceed span/250. Beyond this limit the deflection will give offence to the occupant.
2. The deflection which arises after the construction of the partitions or the application of finishes should not exceed span/350 or 20 mm, whichever is the lesser. In cases where rigid brick walls are used, the deflection should be limited to span/500 or 10 mm. These limitations are provided to avoid damage to partition and finishes
3. In the case where finishes are to be applied to prestressed concrete elements, the total upward deflection of the elements should not exceed span/300.

3. Computational mechanics

3.1 A general approach to kinematics

A general understanding of the kinematics, relating deformed and undeformed configuration of a body was obtained after consulting the work presented by Sack (2014).

Consider a body $\boldsymbol{B}$ in three dimension Euclidean vector space. During analysis, the body will have two states, namely the undeformed state usually referred to as $\boldsymbol{B}$, and a deformed state usually referred to as $\boldsymbol{B}_t$.

The undeformed configuration state, $\boldsymbol{B}$ is a parametised by the Cartesian coordinates X_1, X_2, X_3, where the associated basis vectors are denoted by $\mathbf{e}_1$, $\mathbf{e}_2$, $\mathbf{e}_3$. During analysis, after being subjected to a certain boundary conditions, the body, at time t, in its deformed state is referred to as $\boldsymbol{B}_t$.

In order to describe the mapping between the two states, a non-linear deformation mapping $\varphi : \boldsymbol{B} \rightarrow \boldsymbol{B}_t$ is introduced, which enables us to define a relationship between a material point in the reference configuration $\boldsymbol{X} \in \boldsymbol{B}$ and the current configuration $\boldsymbol{X} \in \boldsymbol{B}_t$:

$$\mathbf{x} = \varphi(\mathbf{X}, t) \qquad \text{and} \qquad \mathbf{X} = \varphi^{-1}(\mathbf{x}, t) \qquad \textit{Equation 3-1}$$

Furthermore, an invertible linear tangent map $\mathbf{F}$, so-called deformation gradient tensor, can be defined as the gradient of φ. Consequently, the change in volume from $\boldsymbol{B}$ *to* $\boldsymbol{B}_t$ can be obtained from the *Jacobian J*, which is the the deterinant of $\mathbf{F}$. This is expressed as follows:

$$J = \det \mathbf{F} = \det(\text{Grad}\, \varphi) > 0 \qquad \textit{Equation 3-2}$$

$\mathbf{F}$ can also be written as

$$\mathbf{F} = \mathbf{1} + \text{Grad}\ \mathbf{u} \qquad \textit{Equation 3-3}$$

where $\mathbf{1}$ is the identity tensor and $\mathbf{u}$ is the displacement field given by $\mathbf{u}(\mathbf{X}, \mathrm{t}) = \mathbf{x}(\mathbf{X}, \mathrm{t}) - \mathbf{X}$.

In the case where there is no deformation, $\mathbf{u} = 0$, leaving $\mathbf{F} = \mathbf{1}$. Substituting this in Equation 3-2 we get : $J = \det\mathbf{F} = 1$.

The reader is directed to Sack (2014) for more knowledge on the kinematics involved.

3.2 Stress measures

Stress is basically defined as the force acting over a surface area. This can be expressed as follows:

$$\sigma = \frac{F}{A} \qquad \textit{Equation 3-4}$$

However, in computational mechanics, this simple term can be reformulated using the *Cauchy stress* principle; stating the limit of the traction vector $\mathbf{t}^{(v)}$ acting on a surface with normal $\boldsymbol{v}$ can be defined by a force Δf acting on a surface element Δa which is part of a cutting plane throughout the $\boldsymbol{B}_t$. The formulation for the traction $\mathbf{t}^{(v)}$ following the *Cauchy stress* principle is as follows:

$$\lim_{\Delta a \to 0} \frac{\Delta f}{\Delta a} = \frac{df}{\Delta a} = \frac{df}{da} = \mathbf{t}^{(v)} \qquad \textit{Equation 3-5}$$

The state of stress at each point $\mathbf{x} \in \boldsymbol{B}_t$ is then introduced by the *Cauchy stress lemma*:

$$\mathbf{t}^{(v)}(\mathbf{x}, t) = \boldsymbol{\sigma}^{T}(\mathbf{x}, t)\boldsymbol{v}(\mathbf{x}, t) \qquad \textit{Equation 3-6}$$

where $\boldsymbol{\sigma}$ is the *Cauchy stress* tensor in the spatial coordinate of $\mathbf{x}$.

The expression in Equation 3-6 can be rearranged into Equation 3-7, where the element surface that is being considered is dA with a unit normal of $\mathbf{n}$.

$$\mathbf{t}^{(n)}(\mathbf{X}, t) = \mathbf{P}(\mathbf{X}, t)\mathbf{n}(\mathbf{X}, t) \qquad \textit{Equation 3-7}$$

where $\mathbf{P}$ is the first *Piola-Kirchoff* stress tensor which is now a function of the coordinate $\mathbf{X}$.

Another stress measure, the second *Piola-Kirchoff* stress tensor, is introduced where it is related to the first *Piola-Kirchoff* through the deformation gradient $\mathbf{F}$. The expression is as follows:

$$\mathbf{P} = \mathbf{FS} \qquad \textit{Equation 3-8}$$

Hence the second *Piola-Kirchoff* stress can be re-written as follows:

$$\mathbf{S} = \mathbf{F}^{-1}\mathbf{P} \qquad \textit{Equation 3-9}$$

3.3 Principle of virtual work and its discretization

According to Skatulla & Sansour (2015), computational solid mechanics has become widely accepted in the analysis of linear and non-linear structural problems of arbitrary geometry, loading, support conditions, material behavior etc. In the case of non-linear problem, the response of the structure can be complex where load-displacement curve can neither be convex nor monotonic in one of both variables i.e. the load and the displacements. With the presence of limit points in the load-displacements curves, the load increment cannot be formulated directly, instead, the loading parameter itself is considered as an unknown which is solved a so-called path-following methods (Skatulla & Sansour, 2015).

This chapter will provide a concise and brief introduction on the path-following method that is already implemented in the in-house modelling software SESKA. "SESKA is a numerical modelling software based on the element free Galerkin method (EFGM) which used moving least square approximations (MLS) on the solution over the domain" (Skatulla & Sansour, 2015). In the case where the user wants further details with regards to the formulation of the path-following methods, the user is directed to the paper by Skatulla & Sansour (2015).

3.3.1 The variational principle and its linearization

Firstly, let's consider a non-linear boundary value problem in the domain of $\boldsymbol{B}$ with the boundary $\partial \boldsymbol{B}$. The Dirichlet boundary conditions are prescribed on $\partial \boldsymbol{B}_D \subset \partial \boldsymbol{B}$ and Neumann boundary conditions are prescribed on $\partial \boldsymbol{B}_N = \partial \boldsymbol{B} / \partial \boldsymbol{B}_D$.

The external virtual work, $\mathrm{W}_{(\mathrm{ext})}$ in the Langrangian form is defined as follows:

$$\mathrm{W}_{(\mathrm{ext})} = \int_{\mathrm{B}} \mathbf{b}.\delta\mathbf{u}\,\mathrm{dV} + \int_{\partial \mathrm{B}_{\mathrm{N}}} \mathbf{t}^{(\mathrm{n})} \cdot \delta\mathbf{u}\,\mathrm{dA} \qquad \textit{Equation 3-10}$$

where $\delta\mathbf{u}$ represents the virtual displacement vector, $\mathbf{b}$ the body force and $\mathbf{t}^{(\mathbf{n})}$ the external traction vector acting on $\boldsymbol{B}_N$. dV represents a volume element of domain $\boldsymbol{B}$ while dA is a surface element of its corresponding boundary $\partial \boldsymbol{B}$ with the outward surface normal vector $\mathbf{n}$.

The *Green strain* tensor can be defined as:

$$\mathbf{E} = \frac{1}{2}(\mathbf{F}^{\mathbf{T}}\mathbf{F} - 1) \qquad \textit{Equation 3-11}$$

and elastic right *Cauchy-Green* deformation tensor as:

$$\mathbf{C} = \mathbf{F}^{\mathbf{T}}\mathbf{F} \qquad \textit{Equation 3-12}$$

where **F** is the deformation gradient tensor already defined in Equation 3-3.

With $\psi(\mathbf{C})$ defining the strain stores energy, the variation of the internal potential with respect to **E** in the Lagrangian form is expressed as follows:

$$\psi_{(\text{int})} = \int_B \frac{\partial \psi(\mathbf{C})}{\partial \mathbf{E}} : \delta\mathbf{E}\, dV \qquad \textit{Equation 3-13}$$

Using the first law of thermodynamics, where sum of the external work done from Equation 3-10 and internal work from Equation 3-13 should equate to zero, the following variational statement is obtained:

$$\sum Workdone \; = \psi_{(\text{int})} - W_{(ext)} = 0$$

$$= \int_B \mathbf{S} : \delta\mathbf{E}\, dV - \int_B \mathbf{b}.\delta\mathbf{u}\, dV - \int_{\partial B_N} \mathbf{t}^{(n)} \cdot \delta\mathbf{u}\, dA = 0 \qquad \textit{Equation 3-14}$$

where **S** denotes the second *Piola-Kirchoff* stress tensor given by:

$$\mathbf{S} = \frac{\partial \psi}{\partial \mathbf{E}} \qquad \textit{Equation 3-15}$$

The double dot (:) denotes the scalar product of tensors. The variational principle is supplemented by the so-called Dirichlet boundary conditions:

$$\mathbf{u} = \hat{\mathbf{u}} \text{ on } \partial \mathrm{B}_{\mathrm{D}} \qquad \textit{Equation 3-16}$$

Now, taking in consideration the general case of finite strain and non-linear material behavior, the variational statement obtained in Equation 3-14 above is solved incrementally and iteratively using the *Newton-Raphson* method.

For each iteration step, *i*, of an incremental loading or time step, n, the variational statement is linearized using a first-order Taylor expansion in the vicinity of some known solution of the displacement field. For more in depth explanation on the linearization and convergence solution obtained after each loading step, the user is referred to the paper by Skatulla & Sansour (2015).

3.4 Constitutive Law

In computational analysis, a so-called constitutive model is usually used to provide a mathematical description of how the material respond to various loadings (Buyukozturk & Shareef, 1985). Depending on the type of material, appropriate constitutive models should be used accordingly.

During the past years, significant effort was put in the development of an elastic constitutive model for concrete materials (Lowes, 1999). Hence, two elastic constitutive models are presented in this chapter: a hyperelastic type formulation and a hypoelastic type formulation (Buyukozturk & Shareef, 1985).

There is a widespread use of plasticity theory in the modelling of reinforcing steel bars. This can be explained by the plastic region in the stress-strain curve of reinforcing steel under tensile axial load and the plasticity model can accurately predict such behavior (Lowes, 1999). However, a simpler model can be used if only the linear part of the stress-strain curve is to be modelled. Such model is based on the linear hyperelasticity theory.

3.4.1 Hyperelasticity

According to Ogden (1997), when the stress-strain behavior of an elastic material can be derived completely from a strain-energy function, the material is referred to as hyperelastic material. In the formulation of hyperelastic material models, a simple form of constitutive relation is first introduced (Kim, 2014). Using the St Venant-Kirchhoff stress elastic material, the following strain energy density relationship is considered:

$$W(\mathbf{E}) = \frac{1}{2}\mathbf{E} : \mathbf{D} : \mathbf{E} \qquad \textit{Equation 3-17}$$

where $\mathbf{E}$ is the *Green strain* tensor, the notation ":" is the contraction operator of tensors, such that $\mathbf{a} : \mathbf{b} = a_{ij} b_{ij}$, and $\mathbf{D}$ is the fourth-order constitutive tensor for isotropic materials, defined by

$$\mathbf{D} = \lambda \mathbf{1} \otimes \mathbf{1} + 2\mu \mathbf{I}$$

$$D_{ijkl} = \lambda \delta_{ij} \delta_{kl} + \mu(\delta_{ik} \delta_{jl} + \delta_{il} \delta_{jk}) \quad \textit{Equation 3-18}$$

where λ and μ are Lamé's constants for isotropic materials, **1** is the second-order identity tensor, $\otimes$ is the symbol tensor product, and **I** is the fouth-order unit symmetric tensor. The Lamé's constants can be expressed using regular elastic constants for the isotropic material as

$$\lambda = \frac{vE}{(1+v)(1-2v)} \quad \textit{Equation 3-19}$$

$$\mu = \frac{E}{2(1+v)} \quad \textit{Equation 3-20}$$

where E is the Young's modulus and v is the Poisson's ratio.

Differentiating Equation 3-17 with respect to the *Green strain* tensor **E** gives the constitutive relation for non-linear hyperelastic material:

$$\mathbf{S} \equiv \frac{\partial W(\mathbf{E})}{\partial \mathbf{E}} = \mathbf{D} : \mathbf{E} = \lambda tr(\mathbf{E})\mathbf{1} + 2\mu \mathbf{E} \quad \textit{Equation 3-21}$$

where **S** is the second Piola-Kirchhoff stress (Kim, 2014).

3.4.2 Hypoelasticity

For hypoelastic formulation, the elastic behavior is maintained only for very small strain changes, thus explaining the term "hypo" meaning to a lesser degree. Hence, hypoelastic formulation is only adequate for infinitely small strain increments or changes. Since the response is path independent, the behavior of the material in unloading will differ from that of the loading. However, since the formulation is still classified as elastic, upon unloading, the material will return back to its original geometry, but via a different path (Ottosen & Ristinmaa, 2005).

The following power law was used to represent the response of hypoelastic material to stresses and strain state:

$$\tau = \tau_0 \frac{\sin(\phi\gamma/\gamma_0)}{\sin\phi}, \qquad \text{for } \gamma < \gamma_0 \qquad \textit{Equation 3-22}$$

$$\tau = \tau_0 \left(\frac{\gamma}{\gamma_0}\right)^{\frac{1}{n}}, \qquad \text{for } \gamma > \gamma_0 \qquad \textit{Equation 3-23}$$

where γ_0 is the initial effective yield strain, $\tau_0 = k\gamma_0$ is the corresponding yield stress and ϕ is a parameter which follows the continuity requirements.

3.4.3 Additive anisotropic

According to Sack (2014), materials that exhibit different deformation properties depending on the material direction are called anisotropic. The discussed material laws in section 3.4.1 and section 3.4.2 are all isotopic, i.e. their material properties are independent of the direction in which they are measured (Sack, 2014). There are cases where a material is made up of isotropic and anisotropic material in a composite manner. Examples of such case is reinforced concrete, where the concrete material is modelled to be isotropic while the reinforcement bars is modelled to be anisotropic where it takes tension in only one direction. A material model has recently been implemented by Dr. Skatulla in the in-house structural analysis software SESKA that enables the analysis of composite material, such as reinforced concrete. The material model is based on the work presented by Klinkel, Sansour & Wagner (2005), where an additive anisotropic model was formulated. This chapter, therefore, gives a brief introduction to the additive anisotropic material model.

The second Piola-Kirchhoff stress tensor for a composite material is generally expressed as:

$$\mathbf{S} = \mathbf{S}_{\mathrm{M}} + \sum_{\mathrm{F}=1}^{\mathrm{nF}} \mathbf{S}_{\mathrm{F}} \qquad \textit{Equation 3-24}$$

The expression is comprised of a matrix, denoted by the sub-indices M, and one or more fibre contributions nF, denoted by the sub-indices F.

This approach considers a volume-averaged response of the bulk material. Now bearing that in mind, the stress of the two terms in the expression above is now formulated based on their volume fractions.

The matrix stress is obtained from an elastic strain energy function $\psi(\mathbf{C})$:

$$\mathbf{S}_{\mathrm{M}} = 2n_M \frac{\partial\psi}{\partial\mathbf{C}} \qquad \textit{Equation 3-25}$$

and the fiber stress is formulated in terms of the logarithmic strain along the fibre:

$$\mathbf{S}_{\mathrm{F}} = E_F \frac{1}{2} \ln(\mathrm{C}_{\mathrm{F}})(\mathbf{V}_{\mathrm{F}} \otimes \mathbf{V}_{\mathrm{F}}) \qquad \textit{Equation 3-26}$$

where E_F is the Young's modulus of the fibre, $(\mathrm{C}_{\mathrm{F}}) = \mathbf{C} : (\mathbf{V}_{\mathrm{F}} \otimes \mathbf{V}_{\mathrm{F}})$ is the compenent of the right Cauchy-Green deformation tensor along the fibre direction $\mathbf{V}_{\mathrm{F}}$.

n_m and n_F are the volume fractions of the matrix and fibre material respectively, where

$$n_M + \sum_{F=1}^{nF} n_F = 1 \qquad \textit{Equation 3-27}$$

The reader is directed to Klinkel, Sansour & Wagner (2005) for further details on the additive anisotropic model.

4. Computational analysis

This chapter gives a comprehensive approach to the computational analysis of prestressed concrete using the conventional forward analysis as well as the inverse analysis. The chapter starts with a material calibration section where constitutive laws, already part of SESKA, were calibrated in order to accurately model the stress-strain relationship of concrete, reinforcing steel bars and prestressing steel tendons. Followed by a material modelling section where the calibrated constitutive laws were used to create a model for reinforced concrete as well as a model for prestressed imbedded steel tendon. Finally, two analysis methods were presented whereby forward and inverse analysis were used in the computational analysis of prestressed concrete. A methodology was proposed for the use of the inverse analysis in the context of analysis of prestressed concrete, where validation of the proposed inverse analysis method was based on the result obtained. The computational analysis was performed using the in-house structural analysis software SESKA.

4.1 Material calibration

Although the hyperelastic and hypoelastic formulations described in the previous section can model complex behaviors of a range of materials, it is essential to obtain and adjust material parameters in their mathematical formulation in order to fit real experimental data. In such a way, realistic results will be obtained when using the calibrated material laws. This chapter, therefore, deals with the calibrations of the material laws formulations discussed in section 3.4 to fit concrete and steel material behavior in their application in prestressed concrete.

4.1.1 Concrete

In cases where material laws have a non-linear stress-strain relationship, their behavior cannot be easily predicted, hence material calibration is required. The material law must be calibrated against a set of experimental data so that the stress-strain curve of the material law fits accurately the curve of the experimental data. Such task is not easy to fulfill, and sometimes calibration just cannot be achieved. This chapter, therefore, deals with the calibration of the Neo Hookean hyperelastic material and the hypoelastic material against a set of experimental data for concrete.

4.1.1.1 Experimental data

In the work presented by Ali, Farid & Al-Janabi (1990), an attempt was made in the formulation of a stress-strain relationship for plain concrete in compression. Polynomial equations in the form of a parabola was proposed based on experimental results.

The stress-strain relationship was obtained by conducting a series of compressive tests on six cylinders (150 mm diameter and 300 mm length) each with different concrete mix and water/cement ratio tested at the age of 28days.

Table 4-1: Mean strength for concrete type mixes (Ali, Farid & Al-Janabi, 1990)

Concrete Type	Mix	(W/C) Ratio	Mean Strength (Mpa)
1	1:1:2	0.40	43.5
2	1:1:2	0.45	32.0
3	1:2:4	0.55	27.7
4	1:2.5:3	0.60	25.3
5	1:2.5:3.5	0.66	16.7

Note: The mean strength is the average of the six specimens

In plotting the stress-strain curve for the different experimental sets of data, the following criteria were followed:

1. Curves start at origin, i.e. $\sigma = 0$, $\varepsilon = 0$
2. The slope of the stress-strain curve at the origin is the modulus of elasticity of concrete, i.e. $\frac{d\sigma}{d\varepsilon} = E_c$
3. The point of maximum stress $\sigma = \sigma_0$ at $\varepsilon = \varepsilon_0$, where $\frac{d\sigma}{d\varepsilon} = 0$

Based on the experimental results, a polynomial equation was developed representing the stress-strain relationship of concrete in compression:

$$\frac{\sigma}{\sigma_0} = \frac{1.9\left(\frac{\varepsilon}{\varepsilon_0}\right)}{1 + 0.9\left(\frac{\varepsilon}{\varepsilon_0}\right)^{2.1}}$$

Equation 4-1

It was found that ε_0 and σ_0 are related with the following proposed expression:

$$\varepsilon_0 = 0.000875\,(\sigma_0)^{0.25} \qquad \textit{Equation 4-2}$$

where σ_0 is in N/mm²

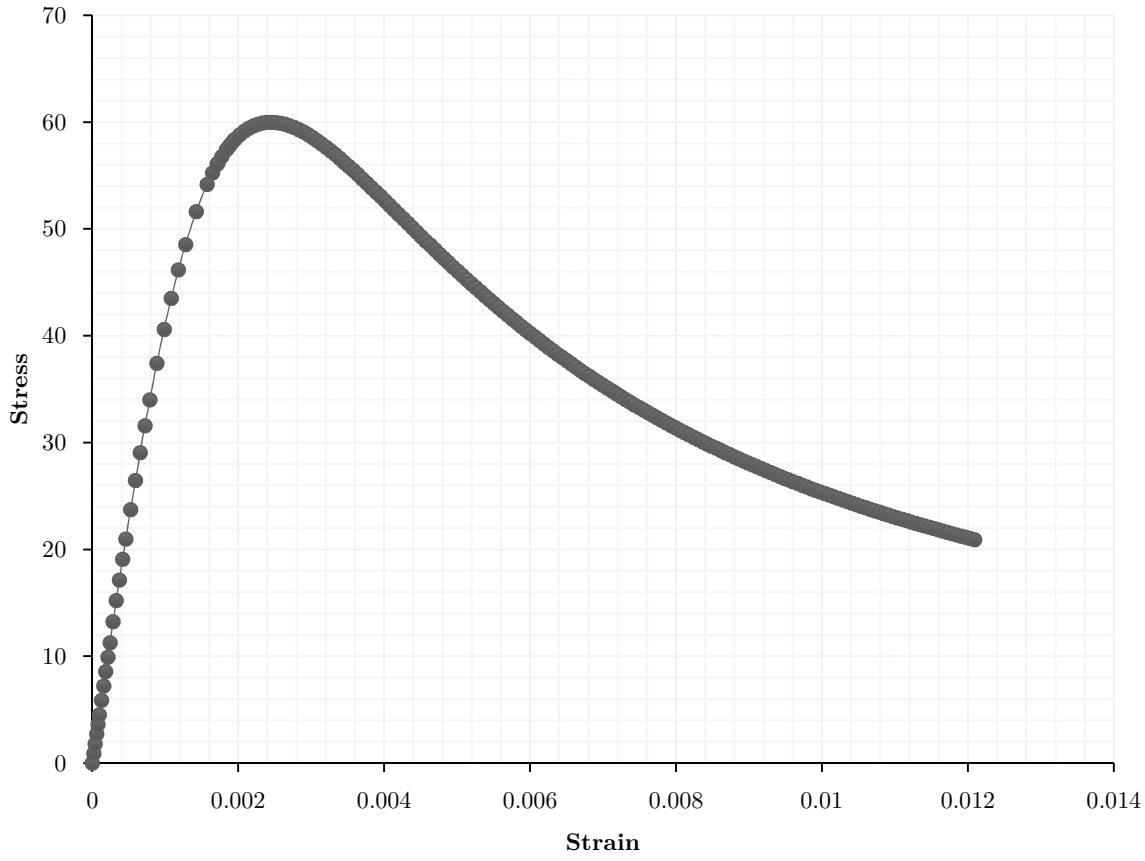

Figure 4-1: Stress strain curve - Experimental data

4.1.1.2 Problem set-up

In this work, the computer modelling was done using the in-house structural analysis software SESKA. In order to accurately calibrate the material law to fit concrete behavior, the modelling was performed under the same conditions similar to the experimental setup discussed above in section 4.1.1.1. Figure 4-2 shows a typical experimental setup that was used to achieve the results obtained by Ali, Farid & Al-Janabi (1990) in section 4.1.1.1.

Figure 4-2: Typical compressive test on cylinder cube (Instron, 2015)

In the problem configuration, a cylindrical model of dimensions 150mm diameter and 300 mm in length under the action of a surface pressure force of 60 MPa was modelled. The problem configuration is shown in Figure 4-3.

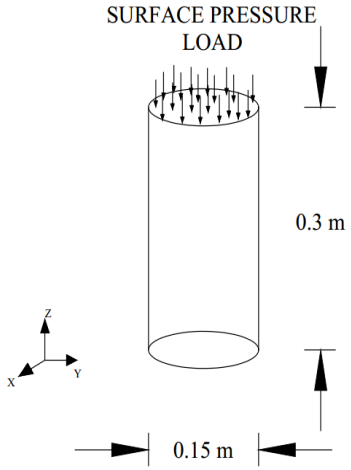

Figure 4-3: Problem configuration

The cylinder model was fixed by setting a displacement surface constraint on the lower surface on the xy plane. This is represented on Figure 4-4 (b). Furthermore, Figure 4-4 (a) show the meshing performed on the cylinder model, and the number of elements meshed in the model can be found in Table 4-2.

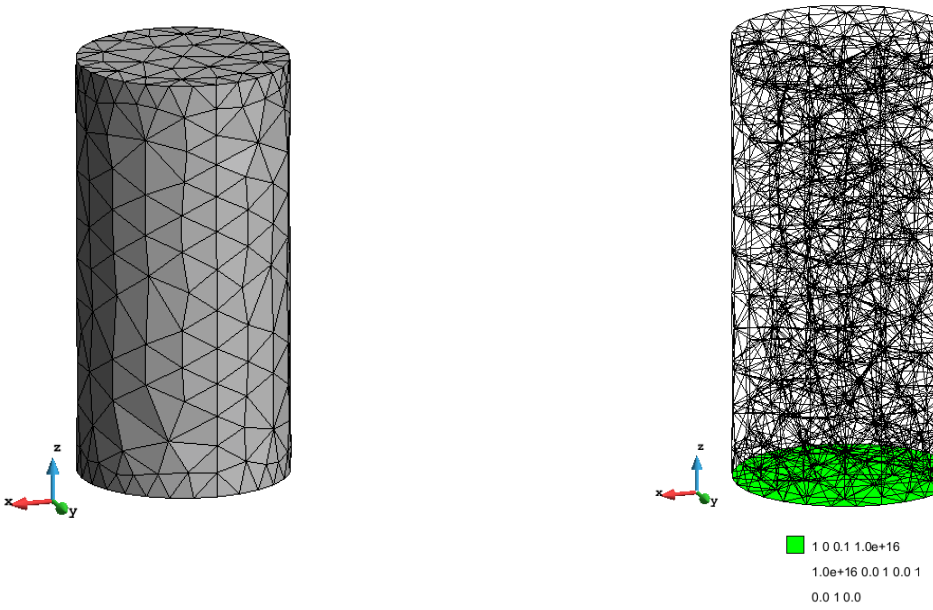

(a) *(b)*

Figure 4-4: Problem setup showing (a) meshing, (b) Dirchlet boundary conditions

Table 4-2: Number of meshed elements

Number of Elements generated	
Number of Triangle elements	580
Number of Tetrahedra elements	2122
Number of nodes	529

4.1.1.3 Fitting Neo Hookean to experimental data

As discussed in section 3.4.1, the Neo Hookean mathematical formulation is dependent on two lamé constants, namely λ and μ. The expressions for both parameters were represented by Equation 3-19 and Equation 3-20.

Compressive test setup as discussed in section 4.1.1.2 was used using Neo-Hookean material. A stress-strain graph was generated for the simulation where the two lamé parameters were varied until the simulation would give a stress-graph of the Neo Hookean material fitting the experimental data. This is shown in Figure 4-5.

The following parameters were used:

Table 4-3: Material parameters - Neo-Hookean

		Units
μ	2.00E+04	MN/m²
λ	8.43E+03	MN/m²

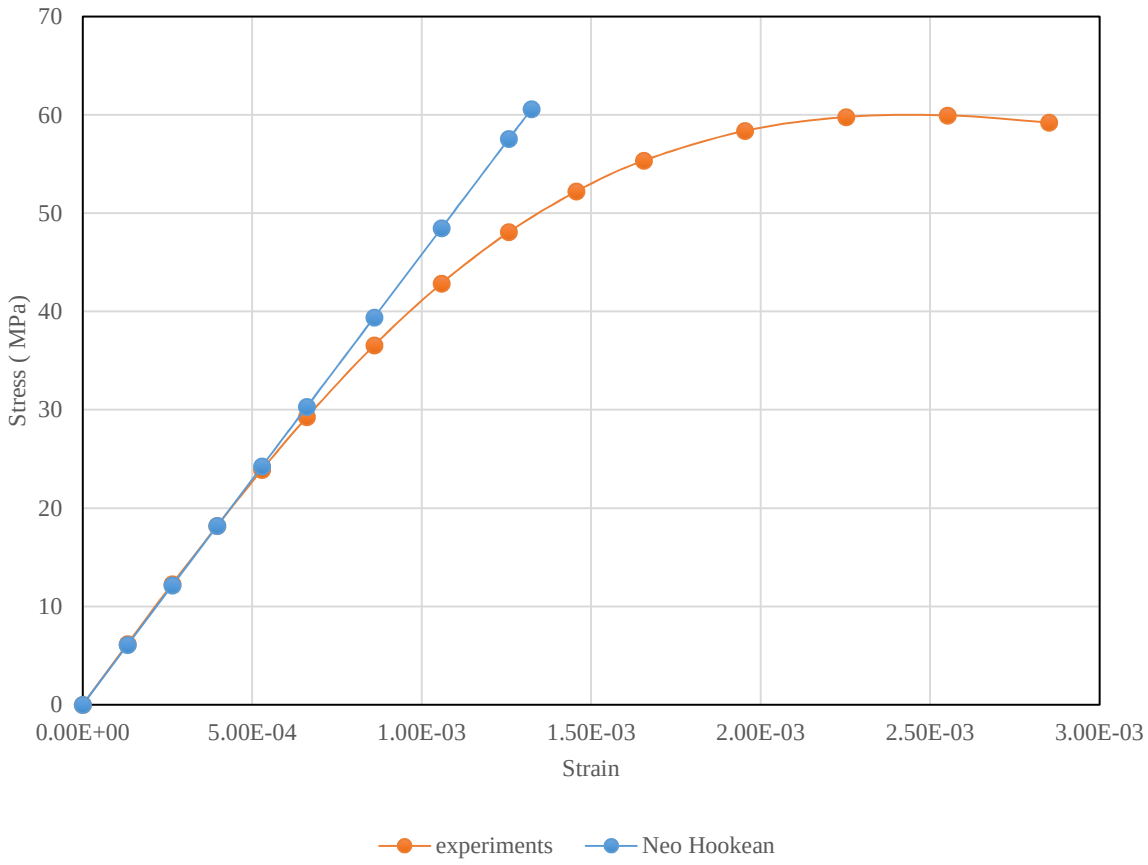

Figure 4-5: Curve fitting - Neo Hookean

The first linear part of the stress-strain curve of the Neo-Hookean material appears to perfectly fit the linear part of that of the experimental data. However, as the stress level increases, the Neo-Hookean curve starts to deviate from that of the experimental data as shown in Figure 4-5. Unless the computational analysis is going to be based on a linear analysis, the use of Neo-Hookean material in the modelling of concrete is deemed to be inaccurate for the purpose of this research project which uses non-linear stress-strain analysis method.

4.1.1.4 Fitting hypoelasticity to experimental data

Similar to section 4.1.1.3, a compressive test modelling was conducted, but this time using hypoelastic material. The power law discussed in section 3.4.2, was used for the calibration process. The key parameters in the power law were varied in the cylinder model in SESKA until the stress-strain curve of the hypoelastic material was found to fit the experimental data. Figure 4-6 shows the graph of obtained for the calibration of the hypoelastic material.

Values for the parameters used are given as follows:

Table 4-4: Material parameters - Hypoelastic

		Units
k	9.44E+03	MN/m^2
n	1.2	-
gamma0	6.35E-03	-
tau0	6.00E+01	MN/m^2

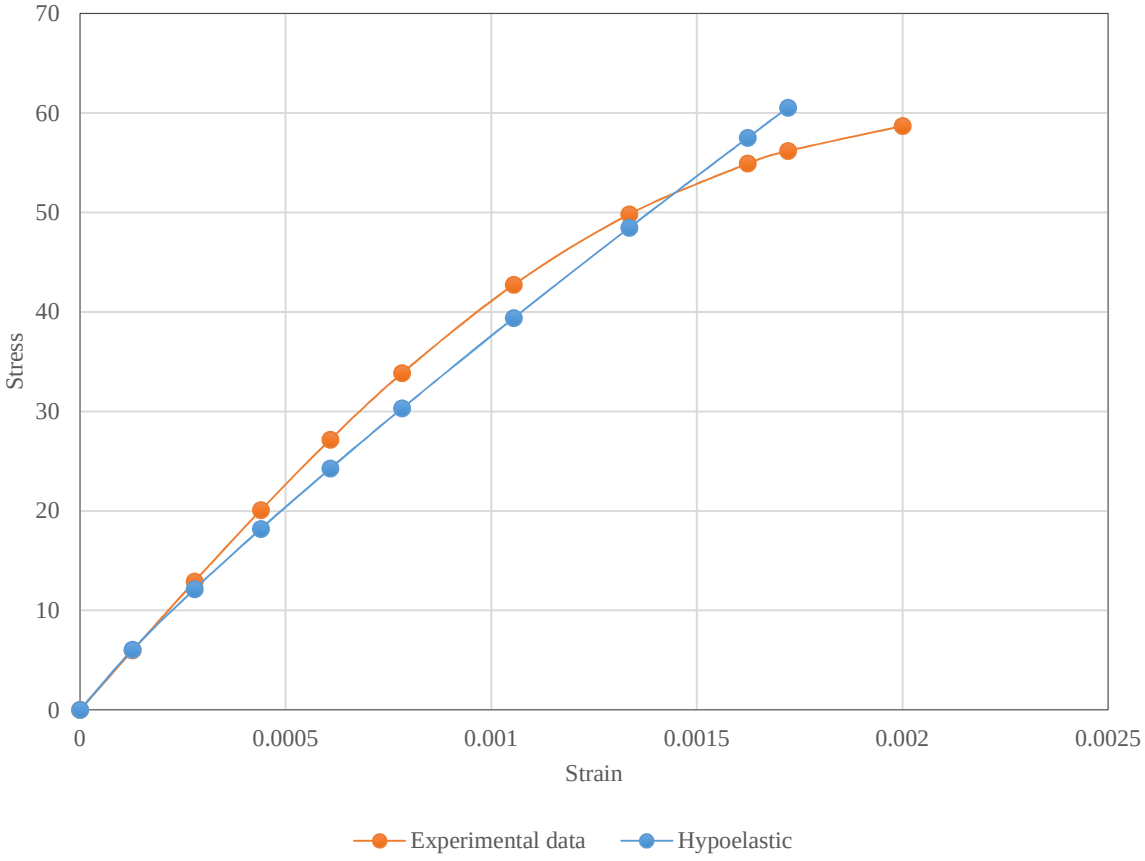

Figure 4-6: Curve fitting - Hypoelastic

The stress-strain graph obtained from the hypoelastic material law was found to fit to a certain degree the experimental data. The initial tangent for both the experimental data and the hypoelastic material seems to fit each other perfectly. However, with increasing stress level, there's a certain degree of discrepancy between the two sets of data. Although it is not a perfect match, the curve fitting was deemed to be satisfactory, and hence the calibrated hypoelastic material law can be said to accurately predict the behavior of concrete under compression. However, the hypoelastic material should be used with care during analysis, as beyond a certain threshold value of 60 MPa, the two curves tend to diverge from each other, where the hypoelastic curve no longer reflect the behavior of concrete. Hence, the calibration is only valid for a maximum compressive strength of 60 MPa.

4.1.2 Reinforced steel bars and steel tendons.

Simple material laws that have a linear stress-strain relationship such as linear hyperelastic constitutive model are quite straight forward to calibrate, since the only parameters required are the young modulus and the poisson ratio which can be obtained from design codes guidelines. Therefore, considering the linear part of the reinforcing steel bars and steel tendon, linear hyperelastic material law was used in their modelling. The parameters for the material was obtained from BS 5400 where a young modulus of 200 kN/mm^2 and poisson ratio of 0.3 was used for both reinforced steel bars and steel tendons as shown in Table 4-5 (BS5400-4-1990).

Table 4-5: Material Parameters - Linear hyperelastic

		Units
E	200E+03	MN/m^2
v	0.3	-

4.2 Material modelling

4.2.1 Concrete and reinforcing steel

The model used was Cauchy isotropy and an additive anisotropic model. The isotropy model was plain concrete and it was used in the middle portion of beam as shown in Figure 4-7. For the modelling exercise, it was decided that no reinforcement will be provided in that area. An additive model consisting of isotropic hypoelastic material and anisotropy linear hyperelastic material was used to represent reinforced concrete. As shown in Figure 4-7, the additive anisotropic model was only used in the top area of the beam structure. This was placed strategically in order to limit cracking caused by tensile stresses that usually develop in that region from hogging moment.

The material laws used for the isotropic concrete material and the anisotropic steel reinforcing bars was developed in section 3.4. The anisotropic material model for steel are oriented in such as way so that it will withstand tension only in the z axis as shown in Figure 4-7. The percentage reinforcing steel used in the model was 1 % of the material volume.

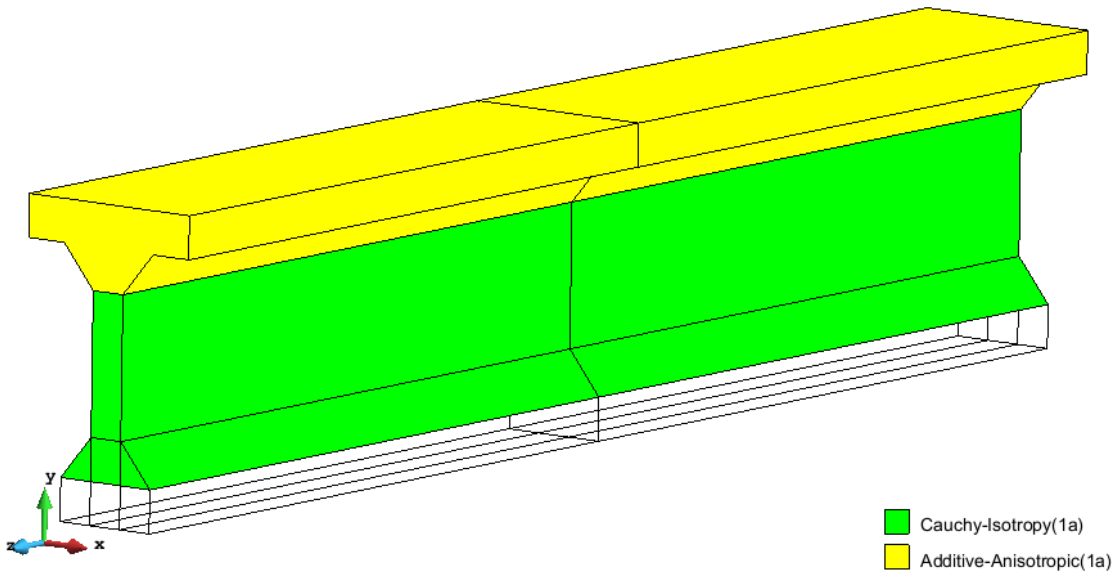

Figure 4-7: Proposed additive model for beam structure

4.2.2 Steel tendon

In the modelling of prestress force, it is important to understand how the prestress steel tendon are arranged in the concrete structure. Steel tendons generally are made up of strands elements, which vary in size and obviously in ultimate tensile strength. According to Benaim (2008), a useful rule of thumb for preliminary design is to assume a working stress of 1000 MPa for the strand. Hence a strand of 13 mm, with an area of 100 mm^2, can take up a force of 100 kN. Furthermore, a strand of 15 mm, with an area of about 150 mm^2 can take up a force of 150 kN. Strands are usually arranged into tendons by making use of anchorage system technology. Anchorage equipment usually varies with manufacturers, hence brochures are usually consulted when determining which anchorage system to be used. Figure 4-8, Figure 4-9 and Figure 4-10 show typical prestress anchors used in the UK. For this calculation example, the CCL prestressed anchor illustrated in Figure 4-10 is used. The tendon that is formed from the prestress anchor can take 37 No. 15.7 mm strands. Therefore, if the prestress force is 10 MN, this will represent 66 strands, hence 2 steel tendons of CCL anchor type will be required.

Figure 4-8: Typical prestress achors: CCL anchor for 6 strands (Benaim, 2008)

Figure 4-9: Typical prestress achors: CCL anchor for 19 No. 15.7 mm strands (Benaim, 2008)

Figure 4-10:Typical prestress anchors: CCL anchor for 37 No. 15.7 mm strands (Benaim, 2008)

The type of prestress anchors used will depend on the prestressing force that is required in the structure. A smaller prestress anchor type will obviously be chosen in cases where the magnitude of the prestress force is low, and while a bigger prestress anchor

type will be chosen when high prestress force is used. An example of arrangement of steel tendons is illustrated in Figure 4-11.

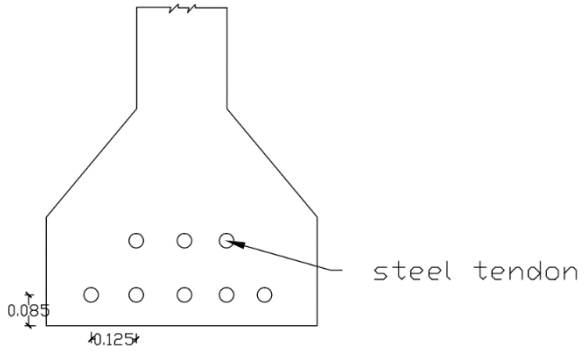

Figure 4-11: An example of a typical arrangement of steel tendons

In the modelling of the prestress force via the steel tendon, a prestress body force model was adopted. The area upon which the prestress body force will be acting will essentially be the area where most of the prestressing steel tendon are located. In the model used for this computational example, the area is the lower part of the I beam where all the steel tendon are located. To be as accurate as possible, the prestress body force was modelled in such a way that the force was made to be a function of the area occupied by the steel tendon on the cross section. Moreover, in the modelling, steel tendons are assumed to have a straight profile. The prestressed body force model is illustrated in Figure 4-12. The material model used for region containing the steel tendon was modelled as additive anisotropic similar to section 4.2.1, the only difference is that the anisotropic material represents the steel tendon.

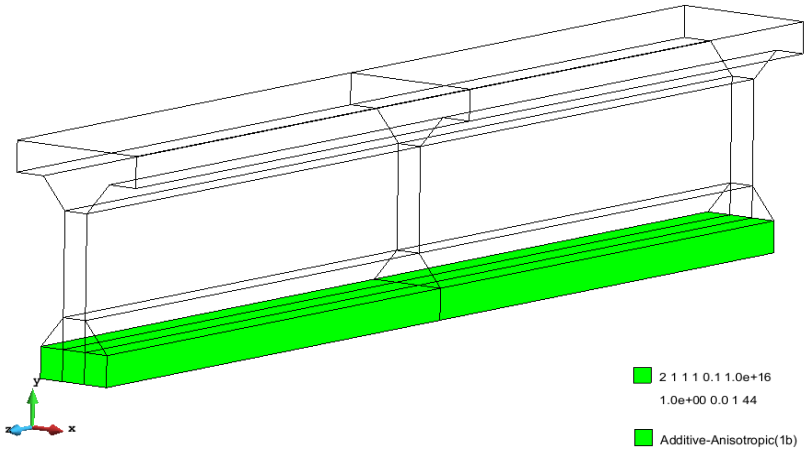

Figure 4-12: Prestress body force and anisotropic material model 1(b)

4.3 Problem set up

For the computational example, a prestressed I beam member from a beam-and-slab bridges was used. The members are precast post-tensioned members where they are made in casting yards, and erected on site with the help of lifting equipment such as cranes. The members are usually placed on bearing supports where they are simply supported. Once the member is in place, concrete slabs are casted in situ on top them to form the bridge structure. A general arrangement of the overall setup is shown in Figure 4-13. Furthermore, Figure 4-14 shows the problem configuration of the prestressed I beam where the beam is made to be simply supported over a length of 10 m.

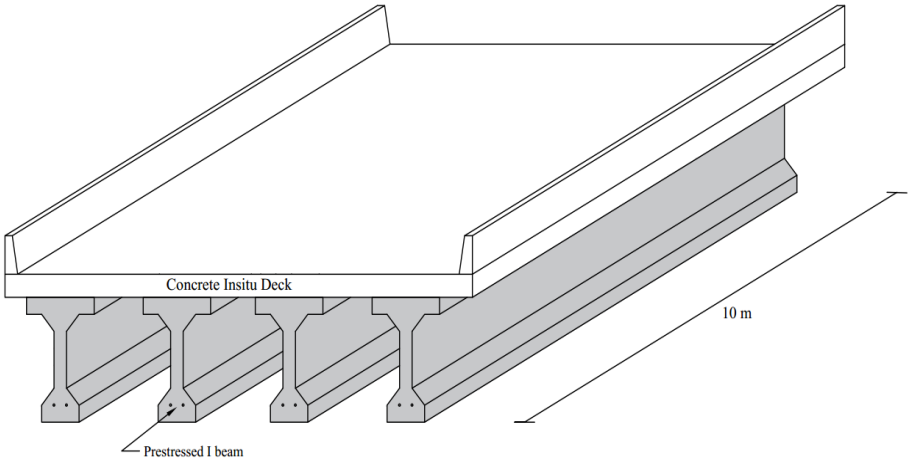

Figure 4-13: Overall Bridge setup

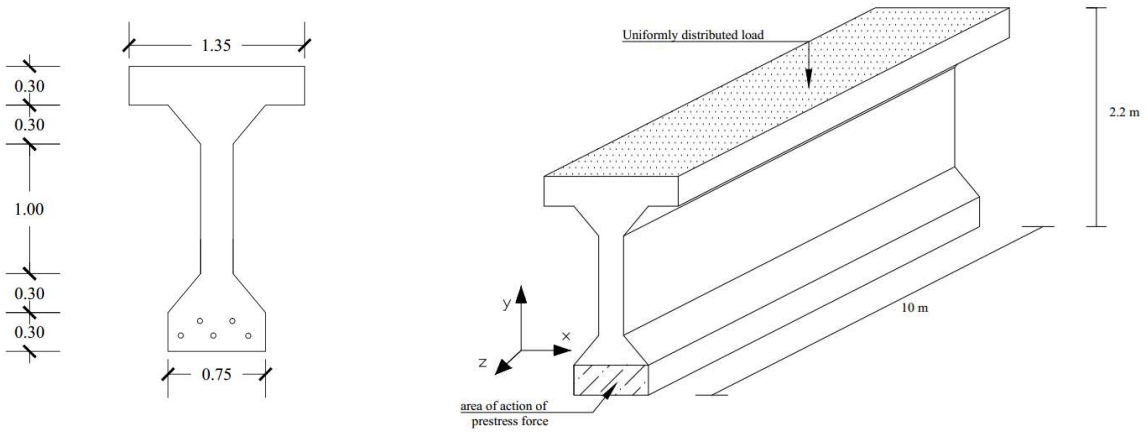

(a) *(b)*

Figure 4-14: Problem setup: (a) Cross section of the I beam, (b) Problem configuration of the I beam

4.3.1 Meshing

The beam was meshed using a mesh size of 0.4 over the entire beam. The meshed beam is shown in Figure 4-15, and the details on the number of element meshed is given in Table 4-6.

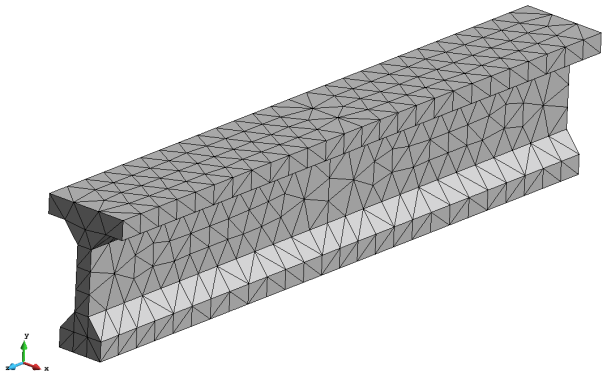

Figure 4-15: Meshed undeformed configuration

Table 4-6: Number of meshed elements

Number of Elements generated	
Number of Linear elements	89
Number of Triangle elements	52
Number of Tetrahedra elements	2304
Number of nodes	722

4.3.2 Boundary conditions

Furthermore, the beam was made to be simply supported by having displacement line-constraints at both ends of the beam; one line was fixed in the y and z axis while the other was fixed only in the y axis. The displacement line-constraints are represented in Figure 4-16(a). A further boundary condition was needed to prevent the beam from moving in the x axis; this was achieved by placing a displacement point-constraint on the edge of the beam as shown in Figure 4-16(b).

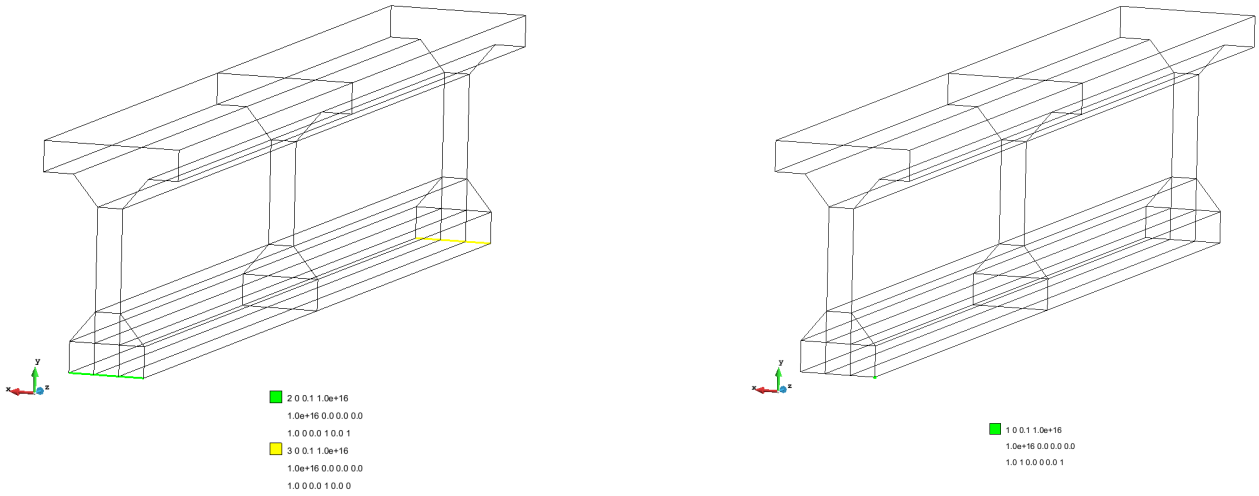

(a) (b)

Figure 4-16: Boundary conditions: (a) Displacement line-constraints, (b) Displacement point constraint

4.3.3 Design load

The dead load the beam has to carry is its own self weight as well as a superimposed load of 100 mm concrete deck lying on top of the prestressed concrete structure. For the analysis example, the only live load that will be considered will be HA loading. HA loading is the normal distributed loading that covers vehicles up to 44 tons. According to the BS 5400-2: 1978, one type of HA loading consist of uniformly distributed load. The UDL for HA loading shall be taken as 30 KN/m along the span of the beam. (BS 5400-2-1978, Clause 6.2) Additionally, pedestrian live load of 5.0 KN/m^2 was also considered. (BS 5400-2-1978, Clause 7.1.1).

In the next section 4.4, more details are provided on how the different load were modelled in SESKA at different stages.

4.4 Analysis method

The construction process of prestressed structures is complex, considering the different stages the structure must go through; from basic structure to the complete structure. During the whole construction period, the structure shape, topology, stiffness, boundary conditions and load conditions are changing with time (Shuenn-Yih Chang, 2012). Design codes usually adopts a forward analysis approach in determining the stress level and shapes of the structure during the different construction stages. The procedure consists of starting with the known initial state of the concrete when it is cast in industry, and the analysis is usually done in accordance with the construction stages. However, in computational analysis, forward analysis can present some limitations with regards in achieving a desired state of the final structure as per design

drawing (Tan, Yu & Zhang, 2012). In an attempt to resolve this limitation, a so-called backward/inverse analysis can be used. The process consists of taking the final desired deformed shape of the structure as its starting point and the process is worked backward up to the undeformed state. In doing so, unknown parameters of the undeformed state such as prestressed forces in the steel tendon can be determined. This chapter gives a background of both forward and backward analysis in the computational analysis of prestressed concrete.

4.4.1 Forward analysis

According to Rajagopal et al., (2007), given as input a set of loading conditions and material properties, the prediction of a deformed configuration of a body can be modelled using computational analysis based on finite deformation elastic theory. This is the so-called forward analysis. In the mentioned work, this application was used in biomedical fields, however, the same concept can be used in concrete modelling since concrete material obeys the same elasticity physical law.

Similar work was also conducted by Grabow (2004), whereby forward analysis was used to analyze prestressed concrete girder in a cable stayed bridge that has to be exposed to construction condition. The analysis was performed in a sequential order from the conceptualization of the structural system in the manufacturing industry to the determination of load factors in each cable. The outcome of the study proved that the forward analysis is reliable since the analysis path coincide with the construction path, hence reflecting reality. In the simulation of prestressed concrete, design codes uses similar principles whereby the prestressed concrete is designed and analyzed in accordance with the construction path of the prestressed concrete structure.

In this chapter, a similar forward analysis approach was used in the computational analysis of the prestressed concrete beam. The analysis was done in accordance with construction stages on the prestressed concrete beam discussed in section 2.7. The simulation was performed on the beam model under the action of prestressed forces, dead load and live load at different stages of the analysis. The beam was modelled as a simply supported beam. For the analysis process, the structure was classified as class 2 where stresses in the prestressed structure at different critical stages were checked against the guidelines set in Table 2-3. Exceeding the prescribed values will see the concrete structure crack in tension and cause certain durability issues. The checks were performed at two construction stages, namely the transfer stage and the SLS (under service) stage.

4.4.1.1 Transfer stage

During the transfer stage, the beam is subjected to the prestressed force and the self-weight dead load. Under these conditions, the hogging moment created by the prestressing force will outweigh the sagging moment of the self-weight dead load, hence the beam element will tend to deflect upwards creating a tension zone at the top fiber and a compression zone at the bottom fiber. The maximum tensile stresses caused by the hogging moment is expected to be experienced at mid span where the bending moment is at its highest. Since the transfer stage is considered to be a critical stage,

it is important to check that the stresses developed in the top and bottom fiber are in accordance with the limitations set in Table 2-3.

The computational analysis was done on a trial and error basis, whereby the prestressed concrete beam was analyzed with different prestressing forces until a suitable range of values for the stresses distribution was obtained.

In the setting up of the loading condition, a prestress body force of 44 MN/m^2 was used to model a prestressing force of 1000 kN. The material model used for the prestress body force has already been discussed in section 4.2.2. Moreover, a traction force of 21.85 kN/m^2 was used to model the action of the self-weight dead load acting on top of the surface of the prestressed concrete beam. The loading configuration model is represented in Figure 4-17.

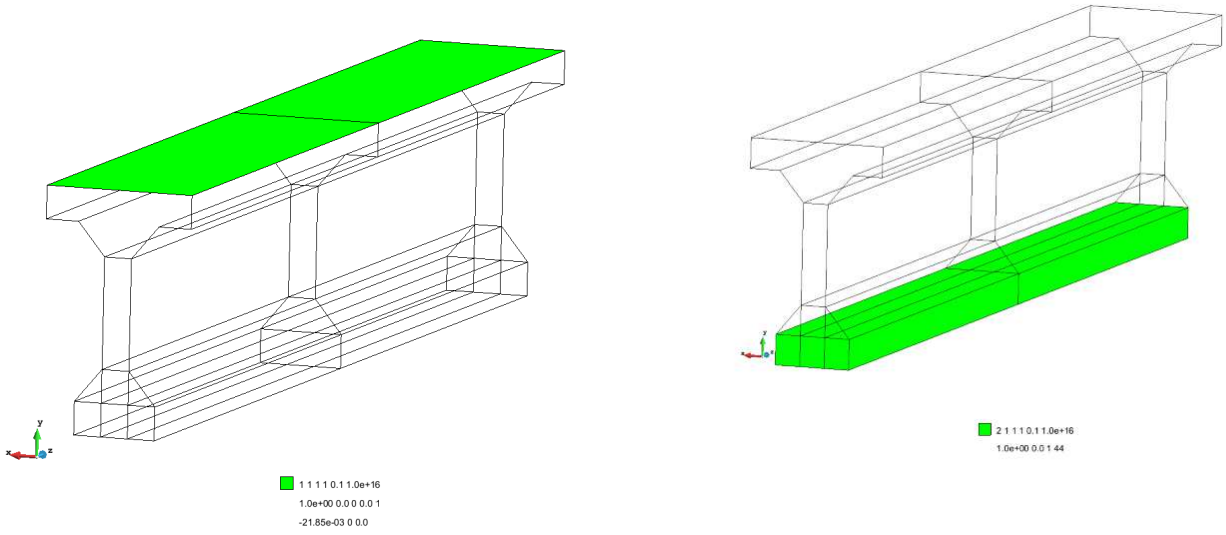

(a) *(b)*

Figure 4-17: Loading conditions: (a) self-weight dead load, (b) prestress body force

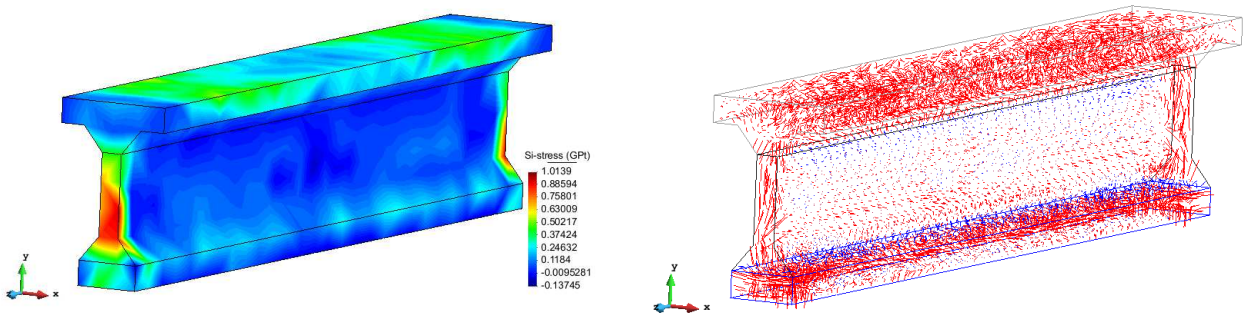

(a) *(b)*

Figure 4-18: Maximum principal stress : (a) Stress contours (MPa), (b) Stress vectors

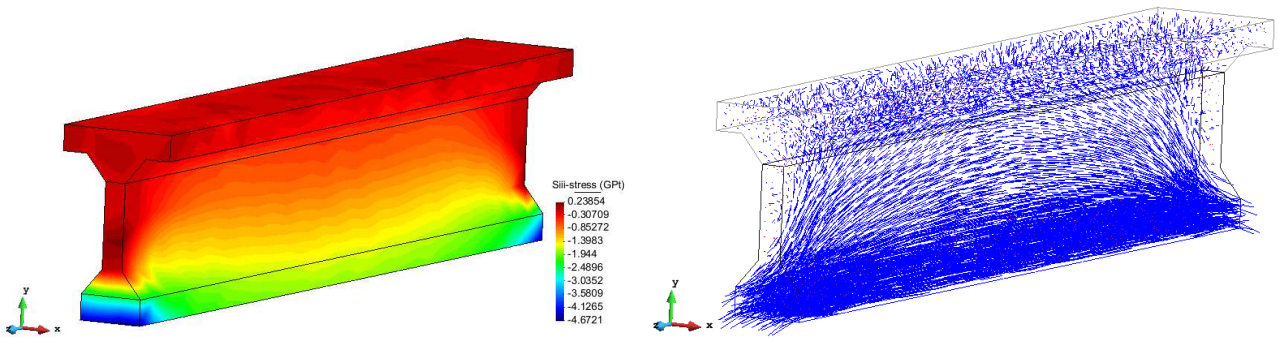

(a) *(b)*

Figure 4-19: Minimum principal stress (a): Stress contours (MPa), (b) Stress vectors

Figure 4-18 and Figure 4-19 shows the princinpal stresses, stress contours and stress vectors, within the beam structure. The stress vectors from Figure 4-18 (b) and Figure 4-19 (b) were generated to obtain a better visualisation of the distribution of the stresses in the structure and the direction at which they are acting.

The distribution of stresses in the bottom fibre of the beam observed in Figure 4-19 (b) accurately describes real life response of prestressing force acting on the anchorage area. For instance, it can be seen that the force vectors from the prestress body force model are transimtted uniformly across the bottom part of the whole structure. A maximum compressive stress of 4.87 MPa was observed in the anchorage area while compressive stress of 1.8 MPa was observed at midspan. The compressive stress at the midspan was found to be lower at middle span due to the effect of the

sagging moment created from the dead load acting on the beam. The sagging moment is at its maximum at middle span, and creates a stress distrubution in the beam cross section at the middle span that would decrease the compressive stress experienced in the bottom fibre. The stress contours from Figure 4-19 (a) gives a good representation of the effect which the sagging moment has on the compressive stress in the bottom fibre of the beam across its whole length.

Now, moving away from the lower part of the structure to the upper part, a general prestress force vector dispersion phenomena can be observed in Figure 4-19 (b). The dispersion can be seen to originate from the area of action of the prestress body force. It is believed that the area of concrete next to the area of compression is subjected to a strain discontinuity creating tensile stresses. This can be observed in Figure 4-18 (a) and (b) where maximum principal stresses can be seen to have developed at the end faces of the beams. Maximum tensile stresses of 1 MPa was observed in that area. Moreoever, from Figure 4-18 (b), it can be see that high tensile stresses are experienced in the top fiber where it reaches value up to 0.58 MPa. The tensile stresses observed in that area are caused by the hogging moment induced from the prestresed force.

Both maximum compressive and tensile stresses were deemed acceptable when checked against guidelines set in section 2.7.

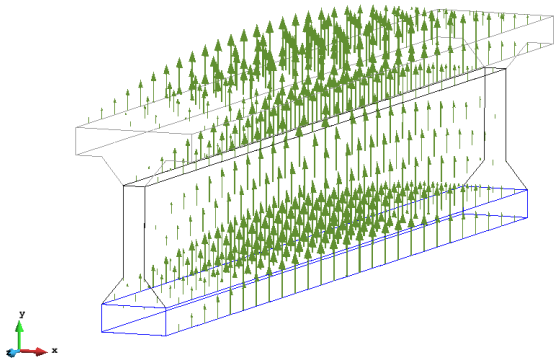

Figure 4-20: Displacement vectors

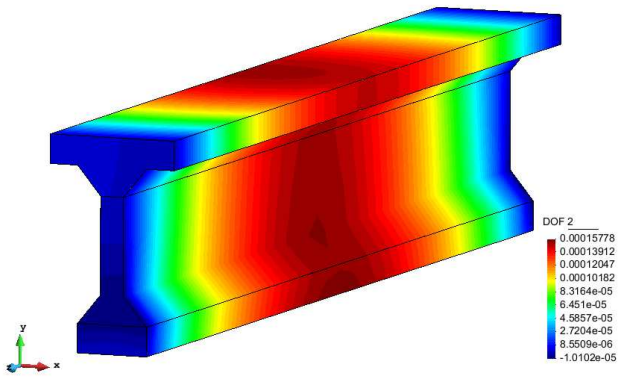

Figure 4-21: Displacement contours (m)

From the displacement vectors in Figure 4-20, it can be seen that the beam structure has a hogging deflection, where maximum deflection is to be foubd at the middle span. The deflection is caused by the hogging moment induced by the prestress forces .From Figure 4-21, the deflection can be seen to be 0.16 mm upward. This 0.16 mm deflection equals to barely no deflection in practical term, and it is believed that the low deflection obtained was due to the high stiffness of the beam section that has a high second moment of area about the x axis. This makes the beam to be very tolerant to high bending moment.

4.4.1.2 SLS stage (Under service)

The next critical stage is when the prestressed concrete is being subjected to maximum service load. The maximum service load will act together with the initial prestressed force and will create a sagging moment that will counteract the hogging moment created by the prestress force. Ideally, the sagging moment and the hogging moment should cancel each other out leaving a prestressed structure with allowable level of compressive and tensile stresses. Similar to the transfer stage, the top and bottom fiber of the deformed structure were checked against Table 2-3.

Normal design practice usually accounts for a certain amount prestress losses in the tendon by the time the structure is being put under service. The losses normally vary along the length of the structure, which render its modelling complex on SESKA. Therefore, in the computational analysis process, no prestress losses were considered.

The loads applied to the prestressed structure during the SLS stage are; the prestressing force of 1000 kN, considering no prestress losses, the self-weight dead load of 21.85 kN/m^2 and a superimposed load of 3 kN/m^2 from the overlying concrete deck and finally a live load of 31.7 kN/m^2 which include HA loading and pedestrian loading. The same loading set up as shown in Figure 4-14 was used, except this time using a total load of 56.55 kN/m^2 as the traction load.

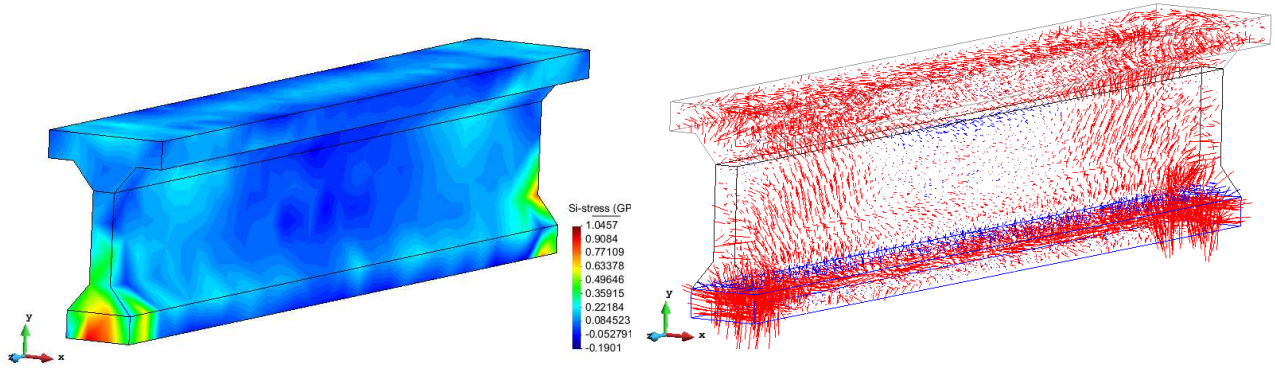

(a) *(b)*

Figure 4-22: Maximum principal stress: Stress contours (MPa), (b) Stress vectors

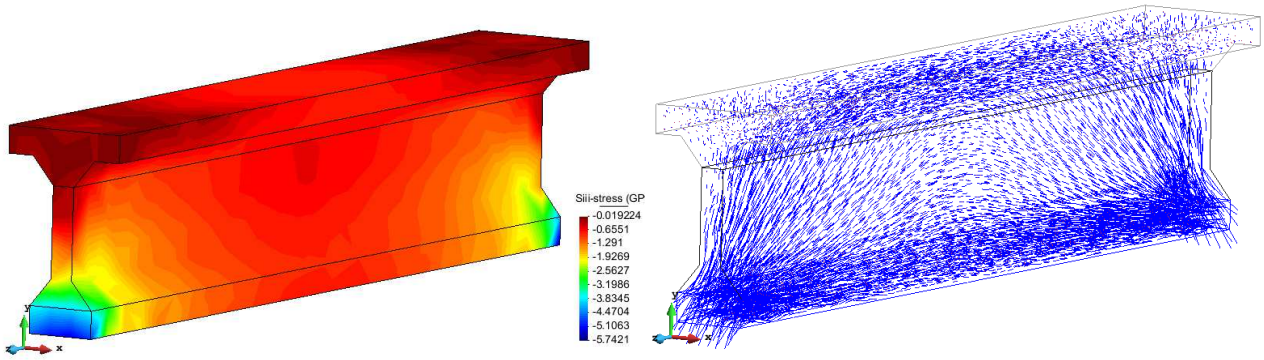

(a) *(b)*

Figure 4-23: Minimum principal stress: (a) Stress contours (MPa), (b) Stress vectors

From Figure 4-22(a), tensile stresses can be observed in the anchorage area of the prestressing steel tendon. For instance, a maximum tensile stress of 0.9 MPa was experienced in that area. It is believed that splitting and bursting forces phenomena described in section 2.6 can be a possible explanation of tensile stresses developed in the anchorage area. Figure 4-22 (b) also gives a clear representation of the tensile stresses experienced in the anchorage area.

In addition to the localised region of high tensile stresses observed in the achorage area, it can also be seen from, Figure 4-23 (a) and (b), a general compressive stress distribution from the achorage area across the whole length of the beam. For instance, maximum compressive stress of 0.15 MPa can be observed at the anchorage area, while a compressive stress of 0.8 MPa can be observed at bottom fibre in at midspan of the structure.

The level of tensile and compressive stresses obtained in the SLS stage were still compliant with the design guidelines set in section 2.7.

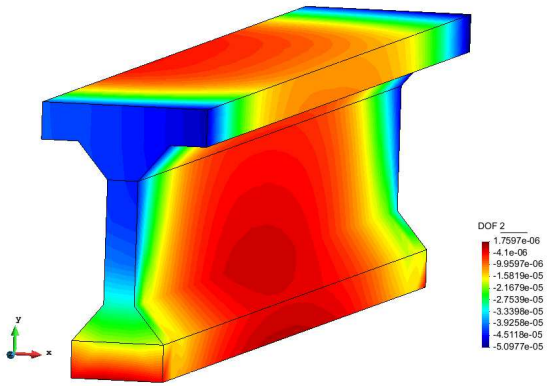

Figure 4-24: Displacements contours (m)

From Figure 4-24, a clear representation of the general behaviour of the structure in its final stage can be observed. The structure has a general downward deflection althouth very minimal. The deflection observed at midspan was to found to be 0.00139 mm downward, which is not noticeable at all.

4.4.2 Inverse analysis

In the work presented by Rajagopal et al., (2007), a formulation of a finite elasticity equations was developed where it is possible to compute a reference state by redefining the knowns and the unknowns in the problem definition. In other words, the undeformed configuration can be determined from the known deformed configuration state of the structure by doing a so-called inverse analysis.

Similar ideology was used in the work presented by Tan, Yu & Zhang (2012), where the undeformed configuration of a prestressed structure was obtained by taking the final deformed shape of the structure as per design drawing as starting point and worked backward. According to Tan, Yu & Zhang (2012), the backward/inverse analysis presented some advantage over forward analysis since forward analysis has certain limitations with regard to achieving desired state of the final structure as per design drawing. Moreover, an inverse analysis was also presented by Grabow (2004) in his construction stage analysis of cable-stayed bridge.

In section 4.4.1, the computational analysis of prestressed concrete was performed using the forward analysis method. In the analysis, the prestress force that is required to produce a safe structure with respect to the design guidelines was determined by trial and error method. The trial and error method was found to be a tedious and time consuming task since computational simulations can take considerable amount of time to run. One way to tackle this limitation is to do as a so-called inverse analysis to obtain a certain unknown parameters to achieve the desired final deformed state of the structure.

In this chapter, a methodology on the use of inverse approach in the analysis of prestressed concrete member is proposed. The analysis was performed on the same beam model developed earlier on in this chapter. In the proposed methodology, the

construction stages used for forward analysis was used in a backward manner. The analysis will start with the deformed shape of the beam in the SLS stage, working backward to the initial unstressed undeformed shape before the prestressed forces are applied. In doing so, the unknown prestress force parameter, which is of interest here, can be determined.

4.4.2.1 Known deformed configuration to unknown deformed configuration

As a starting point for the inverse analysis, the deformed configuration with all the loading cases and boundary condition must be clearly defined. For this example, the deformed configuration of the structure will be taken as a straight member with no deflection at its mid span. This deformed configuration is usually what a designer would ideally want as the final state of the structure. The same loading cases as in the forward analysis were used, but applying it backwards. Figure 4-25 shows the procedure used for step 1. For the inverse analysis, uniform distributed load (Dead load + Live Load) was removed from the deformed structure leaving a cambered deformed structure.

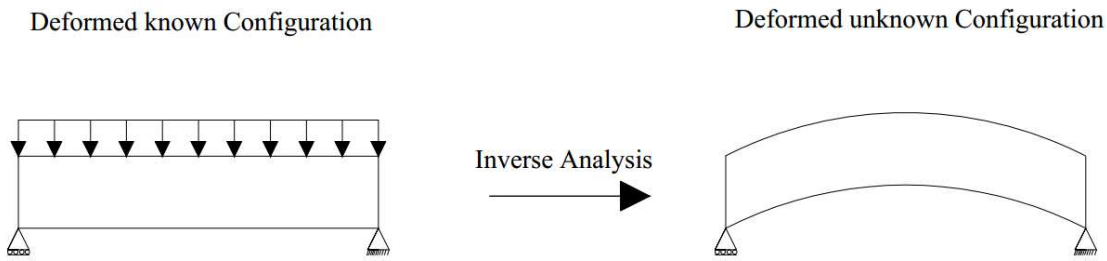

Figure 4-25: Inverse analysis - Step 1

In the inverse analysis, only the geometry of the structure is of concerned, no stress level was checked. The stress level in the structure can only checked in the forward analysis.

A load-deformation graph was generated at a selected node in the middle span of the beam element; the total applied dead and live load was plotted vs the displacement of the node. Figure 4-26 shows the results obtained. The maximum upward deflection obtained was found to be +0.219 mm.

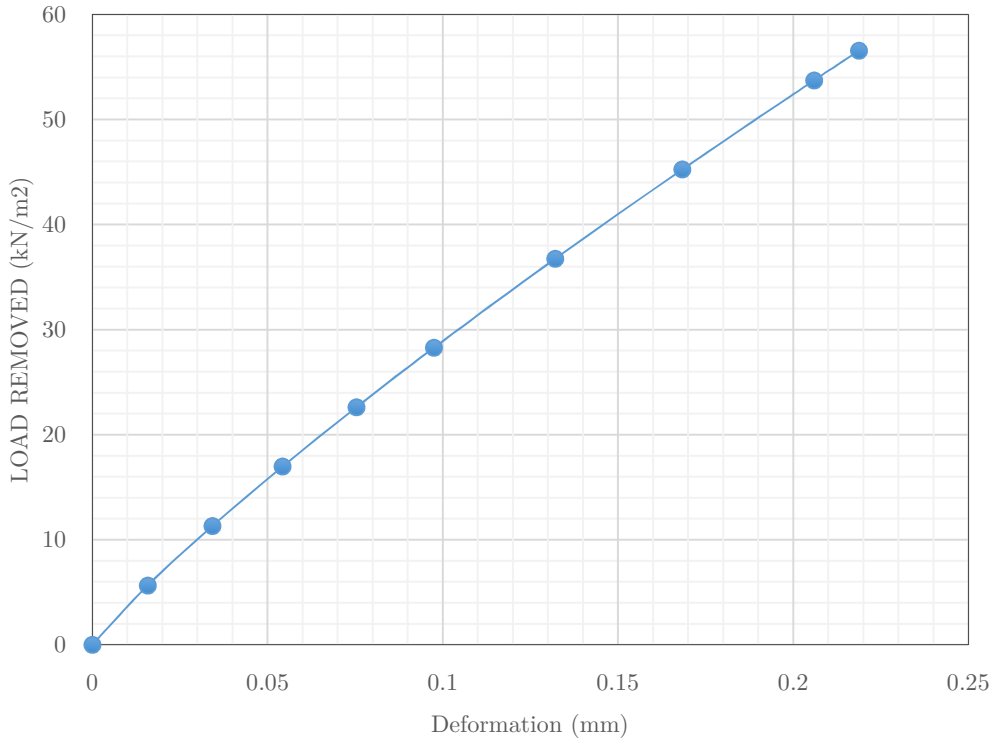

Figure 4-26: Load deformation graph - Step 1

4.4.2.2 Known deformed configuration to known undeformed configuration

In the next step, the unknown deformed configuration obtained from section 4.4.2.1 will now be used as the known configuration in the inverse analysis in this section. As mentioned in section 4.4.2.1, the cambered state obtained is basically the deflection that the prestressed force will cause if it was acting on the concrete on its own. In the proposed inverse analysis method, the deformed configuration of the cambered beam is known from section 4.4.2.1 and the undeformed configuration of the structure before the application of any stresses/forces is also known (i.e. it is an undeflected structure, $\delta = 0$), hence the only unknown parameter that is unknown is the prestress force. In simpler terms, if the deformed shape of the cambered state is known, the prestress force that is required to produce such deflection can be determined. Figure 4-27 shows the procedure to be used for the inverse analysis in this section.

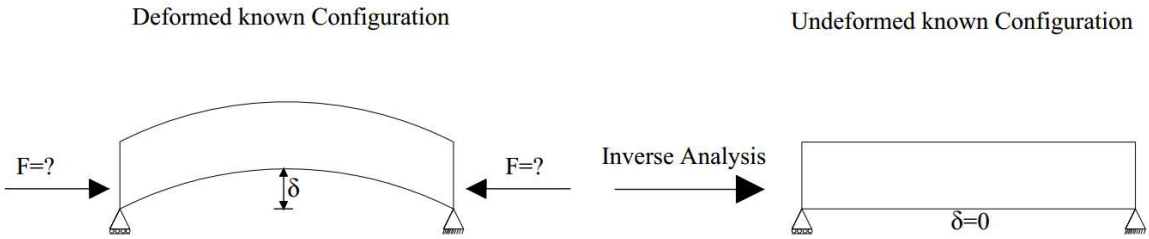

Figure 4-27: Inverse analysis - Step 2

From section 4.4.2.1, the unknown configuration of the cambered structure was obtained, alongside its deflection at the node of interest; where $\delta = +0.219\,mm$ upwards. In this section, a load deflection graph is plotted where the prestressed force is plotted against the displacement at the node. Figure 4-28 shows the generated graph from the simulation. A polynomial equation function represented by Equation 4-3, was associated to the best fit of the curve generated in the load deformation graph, and hence the required prestressed force was calculated by substituting the deflection obtained in section 4.4.2.1, i.e. $\delta = 0.219\,mm$, in the equation. The required prestressed force was found to be 970.5 kN; equivalent to a prestress body force of 43.1 MN/m^2.

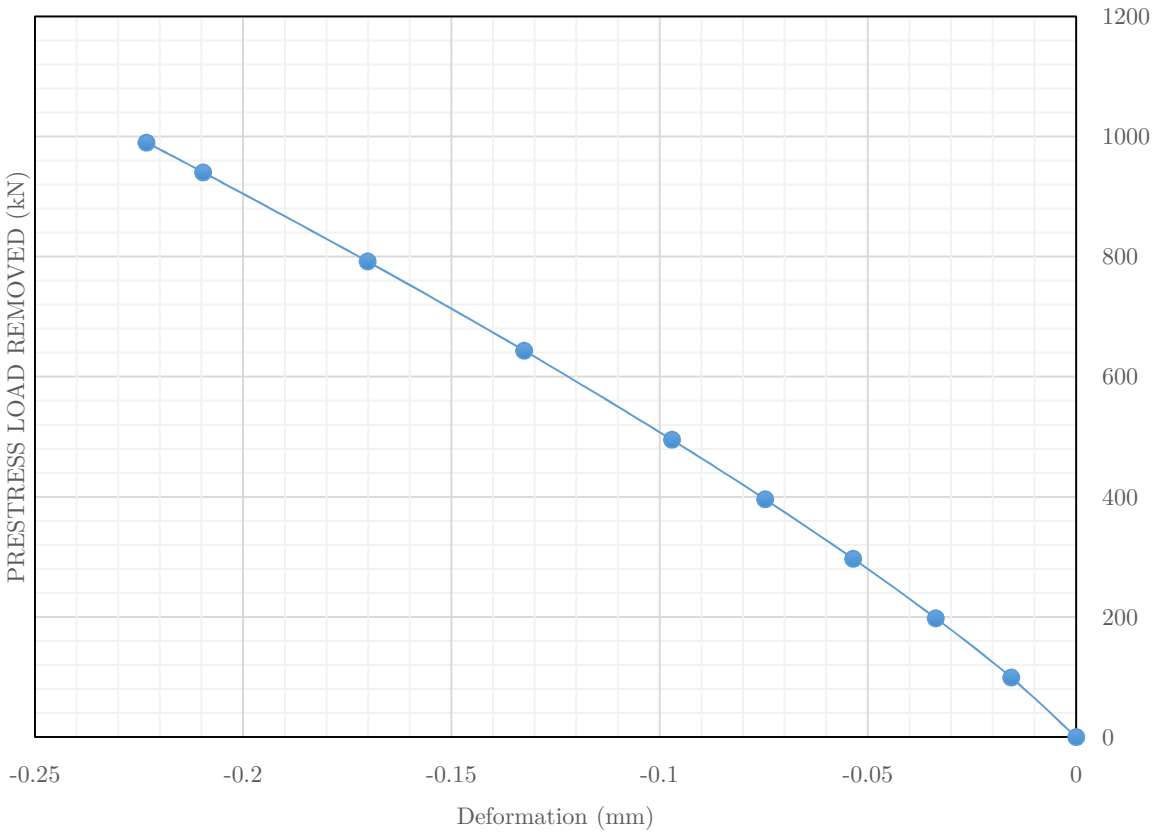

Figure 4-28: Load deformation graph - Step 2

$$y = -5014.3x^2 - 5480x + 11.549$$ *Equation 4-3*

4.4.2.3 Checking final deformed shape

Now that the required prestress forces is obtained, from section 4.4.2.2, it is important to check if the calculated prestress forces will produce a straight member as deformed final shape as predicted by the assumptions made in the inverse analysis. The forward analysis was used in this process. Since this stage is a validation stage for only the geometry of the structure, no stress level was checked in the process.

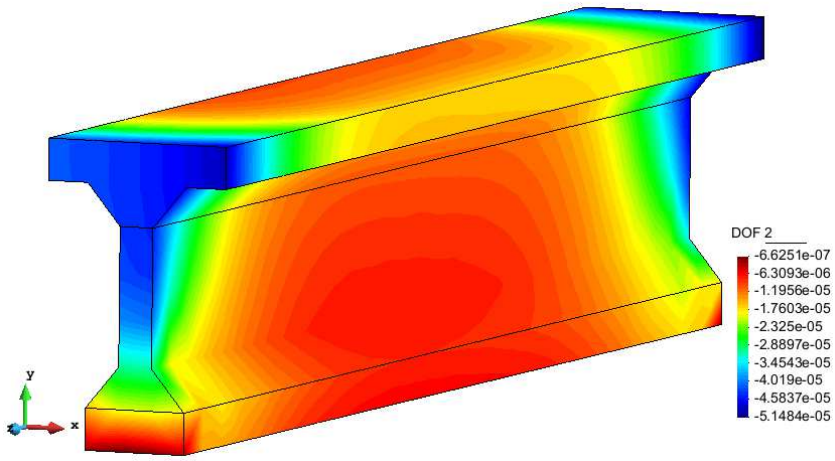

Figure 4-29: Displacement contours (m)

The action of prestress forces along with the all the dead, superimposed and live load produced straight member as shown in Figure 4-29. The level of displacement observed was of magnitude 10^{-5} mm, which is barely noticeably deflection. Hence the use of the inverse analysis can be said to successful.

4.5 Proposed approach

In section 4.4, two computational analysis methods were presented, namely the forward and inverse analysis. The forward analysis enables the analysis of prestressed concrete following the construction stage sequence, where the stress level in the structure could be checked at different critical stages. While the inverse analysis approach proved to be able to predict the final deformed state of the structure, hence in the process, the required prestress force that would produce the desired final deformed state could be determined. In this chapter, a methodology is proposed in using both the inverse and forward analysis together in the computational analysis of prestressed concrete. The proposed approach is illustrated in Figure 4-30.

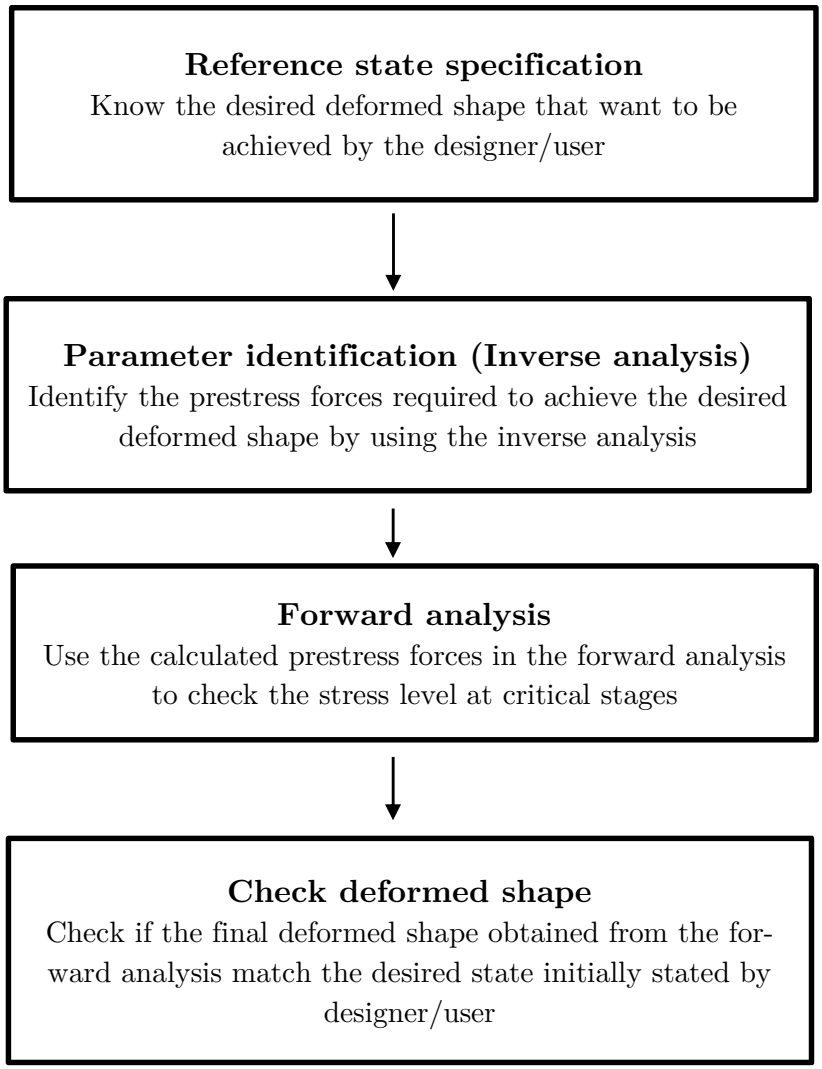

Figure 4-30: Flowchart of the proposed approach

4.6 Concluding remarks

In this chapter, a comprehensive methodology was presented for the modelling and analysis of a prestressed I beam concrete structure.

The results obtained from the material calibration suggested that the use of hypoelastic material in the modelling of concrete was relevant to the study, while the Neo-Hookean material law failed to give conclusive results. Moreover, the simple linear hyperelastic material law was judged to be accurate enough to model for reinforcing steel and prestressing steel tendons.

An additive anisotropic material type was then presented. The additive anisotropic model was used to model for reinforced concrete and concrete containing prestressing steel tendon. The material modelling for prestressing steel tendon imbedded in concrete was further extended to the modelling on how the prestressing steel transfer forces; this was achieved with a prestressing body force model.

With the material laws calibrated and modelling of the concrete presented, two method of computational analysis of prestressed concrete were introduced, namely the forward analysis and the inverse/backward analysis. For the forward analysis method, the results obtained were conclusive to a certain extent since the stress behavior within the prestressed concrete under the action of different forces could be explained and backed up with theories of the principles of prestressed concrete discussed in the literature review. Moreover, the results obtained for the inverse analysis method was also conclusive since the method could accurately predict the shape of the final member.

Following the presentation of the two computational analysis approach, a proposed methodology was presented where it outlined how to make use of both inverse and forward analysis in the computational analysis of prestressed concrete. Now with a proposed method at hand, it will be used to analyze a prestressed concrete structure from a civil engineering case study. For instance, a bridge megastructure was chosen for the analysis as presented in the following chapter.

5. Analysis of full-length precast girder

5.1 Introduction

In section 4, two analysis methods, namely forward and inverse analysis were developed, and the use of the inverse analysis in predicting the final deformed configuration of a structure was validated. The previous prestressed section used in the computational analysis was fairly simple with low level of complexities in its geometry and was made to be simply supported over a rather short distance of 10 m. In order to test the capabilities of both the forward and inverse analysis, in this chapter, computational analysis of prestressed concrete was performed on a real life scenarios of civil engineering megastructure. The prestressed section used in this chapter was chosen from a case study of a bridge megastructure; the Vasco da Gama bridge. An aerial picture of the bridge is shown in Figure 5-1.

Figure 5-1: Vasco da Gama Bridge (PBWORKS, 2011)

The Central Viaduct of the Vasco da Gama Bridge was chosen for the exercise. The Central Viaduct is made up of 77.6 m long simply supported precast box girder units. The sections were made in casting yards on shore, then transported on barges before being lifted on the piers where they are simply supported. A typical cross section of a full-length precast decks is shown in Figure 5-2.

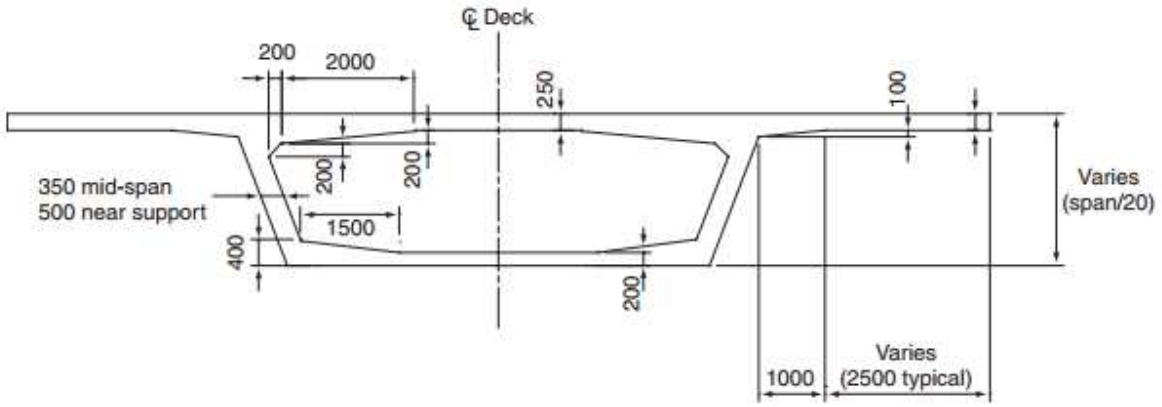

Figure 5-2: Typical single-cell box cross section

5.2 Problem set-up

The proposed section in Figure 5-3 was used in the computational analysis. This structure is inspired from the Central Viaduct part of Vasco de Gama Crossing, hence the beam analysed was made to be simply supported over a length of 70 m. The problem configuration is shown in Figure 5-3.

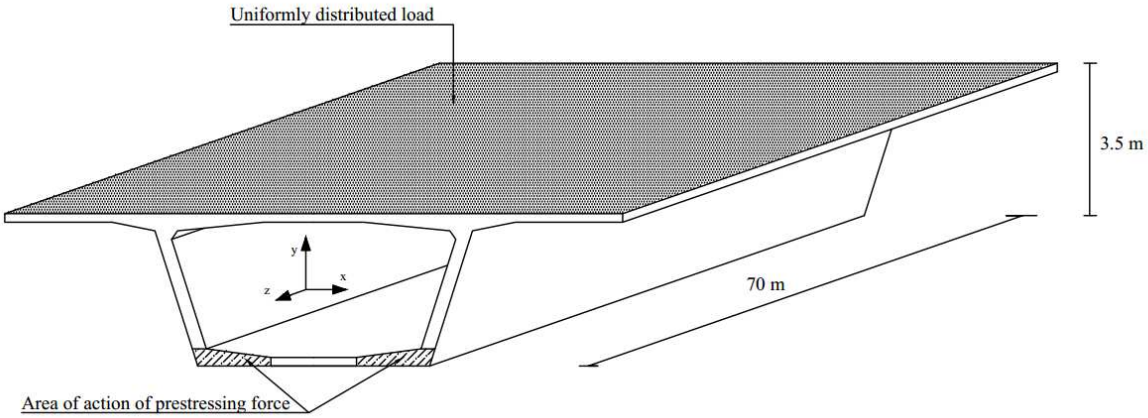

Figure 5-3: Problem configuration of precast box girder

The material modelling of the structure is shown in Figure 5-4. The parameters used for hypoelastic material and linear hyperelastic material in the model is the same of the calibrated material laws performed in section 4.1. As it can be seen in Figure 5-4, the entire structure, except the prestressed area, is modelled as additive anisotropic 1(a), which represents reinforcing concrete with 1% volume of reinforcing steel. The

prestressed area containing the steel tendons is modelled as additive anisotropic 1(b) with 10% volume of steel tendon.

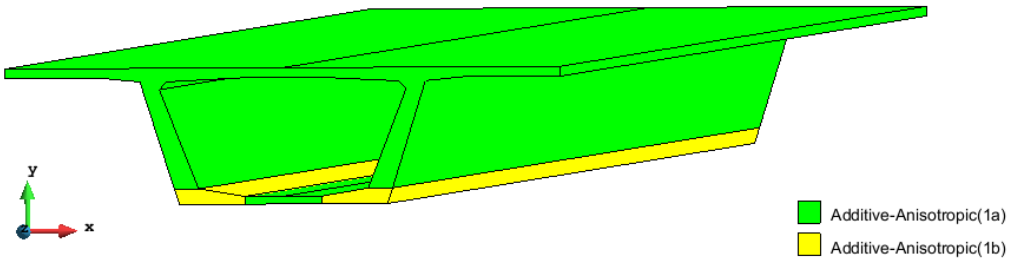

Figure 5-4: Material modelling of the box girder

As mentioned before, the precast box girder is made to be simply supported on the viaduct structure. In the problem configuration, simply supported condition was achieved by having two displacement line-constraint at both lower ends of the beam; one of the line constraint is fixed in both y and z axis, while the other one is only fixed in the y axis. Additionally, a displacement point-constraint condition was placed on one node on the lower right corner of the box girder; the point constraint is fixed in the x axis in order to prevent the structure to move in the x direction during the simulation.

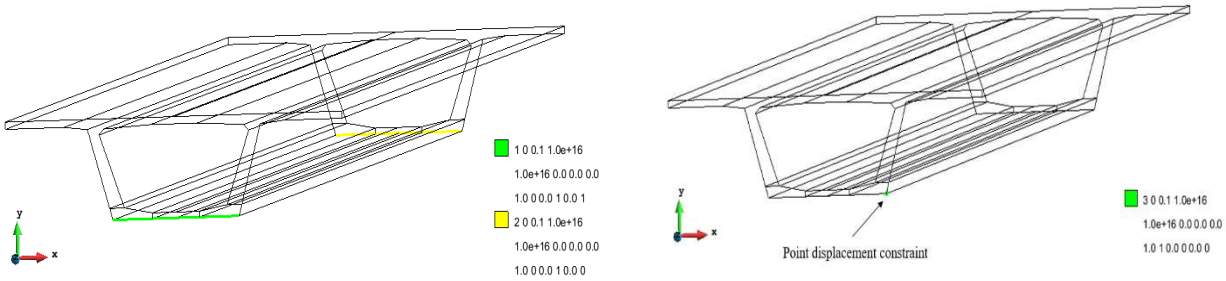

(a) *(b)*

Figure 5-5: Dirichlet boundary conditions: (a) Displacement line constraint, (b) Displacement point constraint

The structure was then meshed as shown in Figure 5-6. The number of mesh elements created is summarized in Table 5-1.

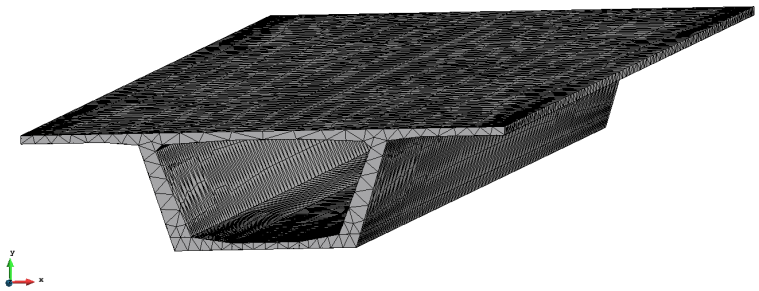

Figure 5-6: Meshed structure

Table 5-1: Number of meshed elements

Number of Elements generated	
Number of Linear elements	2958
Number of Triangle elements	13412
Number of Tetrahedra elements	18896
Number of nodes	6348

There are two types of loading applied to the structure; uniform distributed loads and prestressed forces. The uniform distributed load was modelled by using a surface traction in the y direction acting over the whole upper surface of the structure as shown in Figure 5-3. The calculated dead load and live load were 12.2 kN/m^2 and 10.11 kN/m^2 respectively. Furthermore, the prestressed forces were modelled using a prestress body force acting over the area labelled in Figure 5-3 across the length of the structure. The required prestressed forces are to be determined from the inverse analysis.

In this computational analysis, the method of inverse analysis is first used to determine the prestressing forces necessary to produce a straight member when all the forces are acting in conjunction altogether. This is similar to the methodology used in section 4.5. Once the required load is determined, the stress level in the structure must be checked at the two critical stages of the structure, i.e. at the transfer stage and SLS stage by using the forward analysis. Furthermore, the final deflection of the structure is checked if it complies with the deflection level that was approximated in the inverse analysis.

5.3 Analysis, results and discussion

The methodology used in this analysis in based on the methodology developed in section 4.5.

5.3.1 Step 1: Reference state specification

The final deformed shape that wants to be achieved in this analysis is a straight member with no deflection at its middle span, i.e. $\delta = 0$

5.3.2 Step 2: Inverse analysis

In this step, the unloading of the dead load and live of load was performed on the known deformed configuration. The load deflection graph shown in Figure 5-7 was obtained at a node at the middle span of the structure. The maximum deflection was observed to be 131.3 mm upwards.

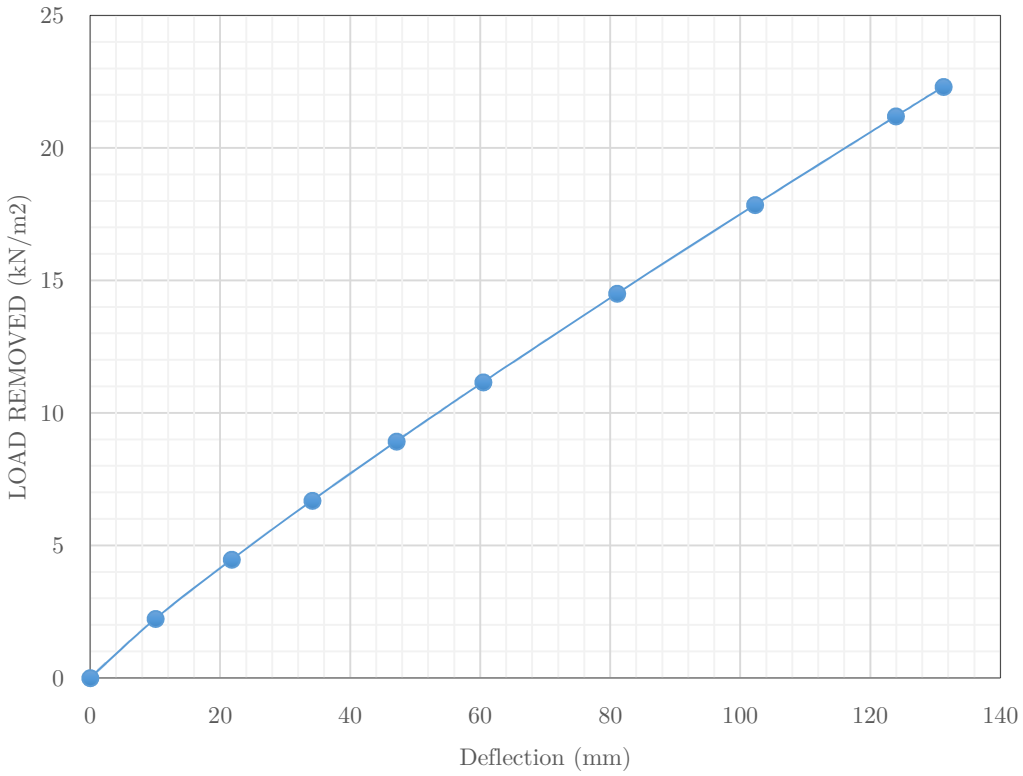

Figure 5-7: Load deflection graph-step1

5.3.3 Step 3: Inverse analysis - determination required prestress force

In the second step of the inverse analysis, reverse loading using the prestress force was performed on the configuration obtained from step 2. A load deflection graph was generated at the same node used in step 2. The graph obtained is shown in Figure 5-8. Subsequently, a polynomial equation function associated to the load deflection graph represented in Equation 5-1 was generated. The prestress force that is required to obtain a straight member was calculated by substituting the deflection obtained in step 2 in Equation 5-1. The required prestress force was found to be 80 MN; equivalent to a body force of 722 MN/m^2.

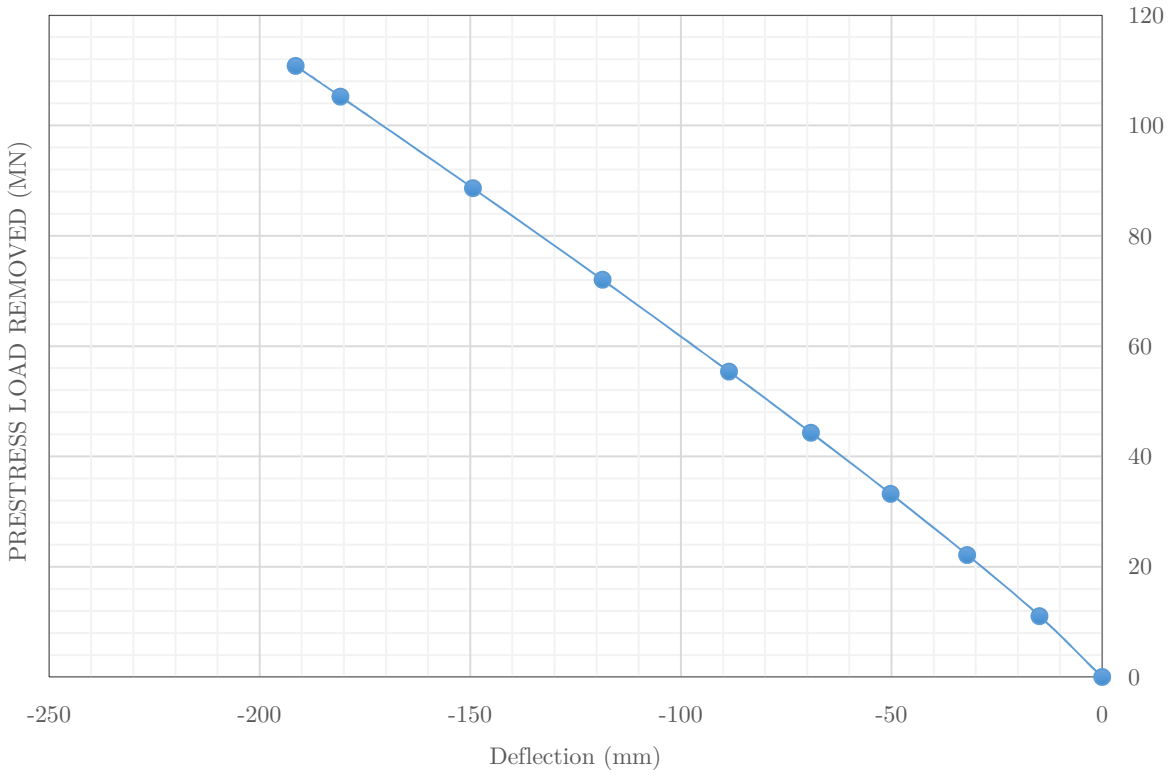

Figure 5-8: Load deflection graph-step 2

$$y = -0.0004\,x^2 - 0.6545\,x + 0.9942 \qquad \textit{Equation 5-1}$$

5.3.4 Step 4: Forward analysis - checking stress level

Now that the required prestress force is obtained from step 3, the stress level at the two critical stages, namely the transfer stage and SLS stage were checked via the forward analysis method.

Transfer stage

Figure 5-9 and Figure 5-10 respectively shows the maximum and minimum principal stresses of the box girder structure. The colour code used in the figures are defined as follows: red colour represents of maximum tensile stress while blue colour represents region of maximum compressive stress.

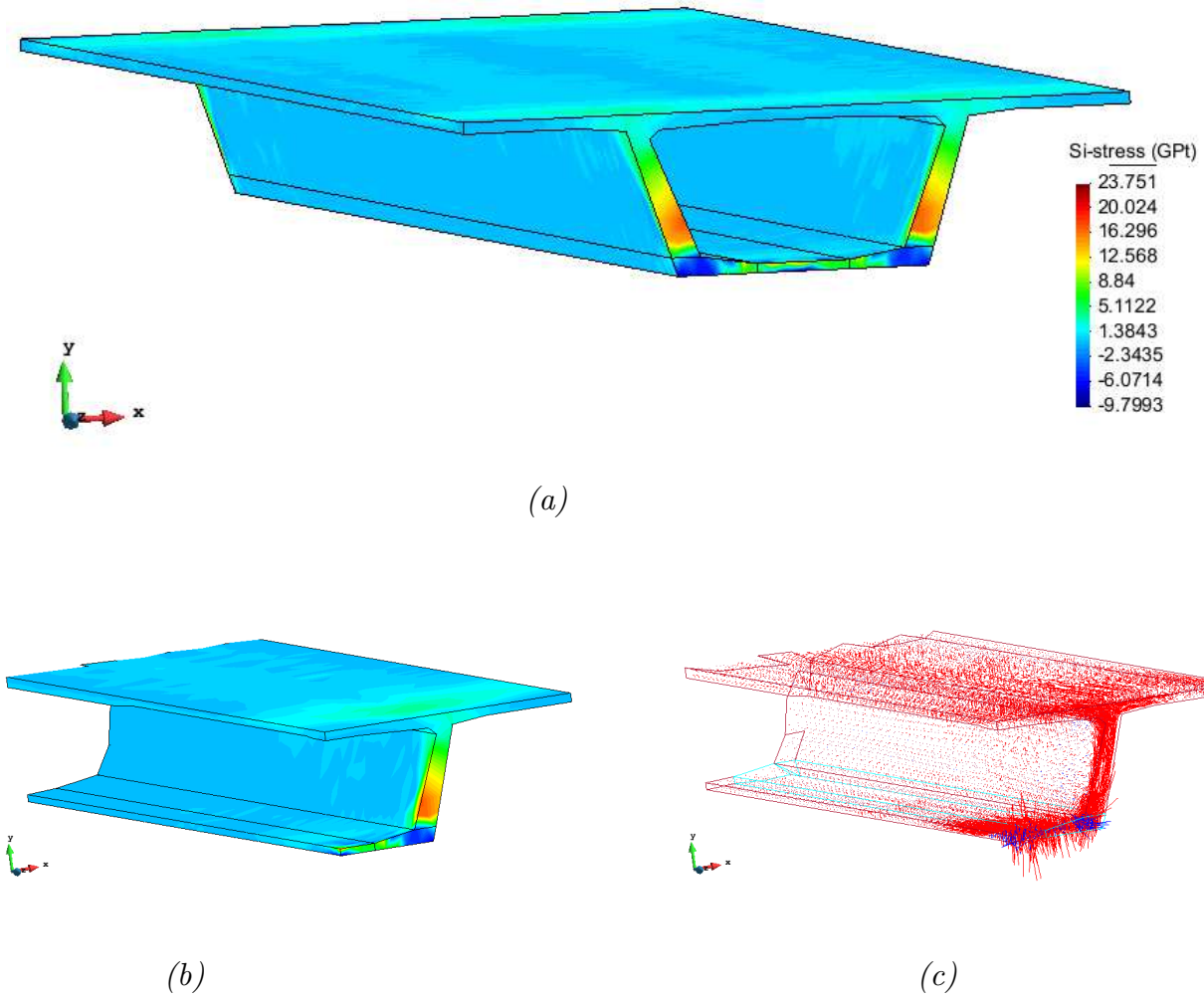

Figure 5-9: Maximum principal stresses: (a) stress contours of full beam (MPa), (b) stress contours of cut beam portion (MPa), (c) stress vectors of cut beam portion

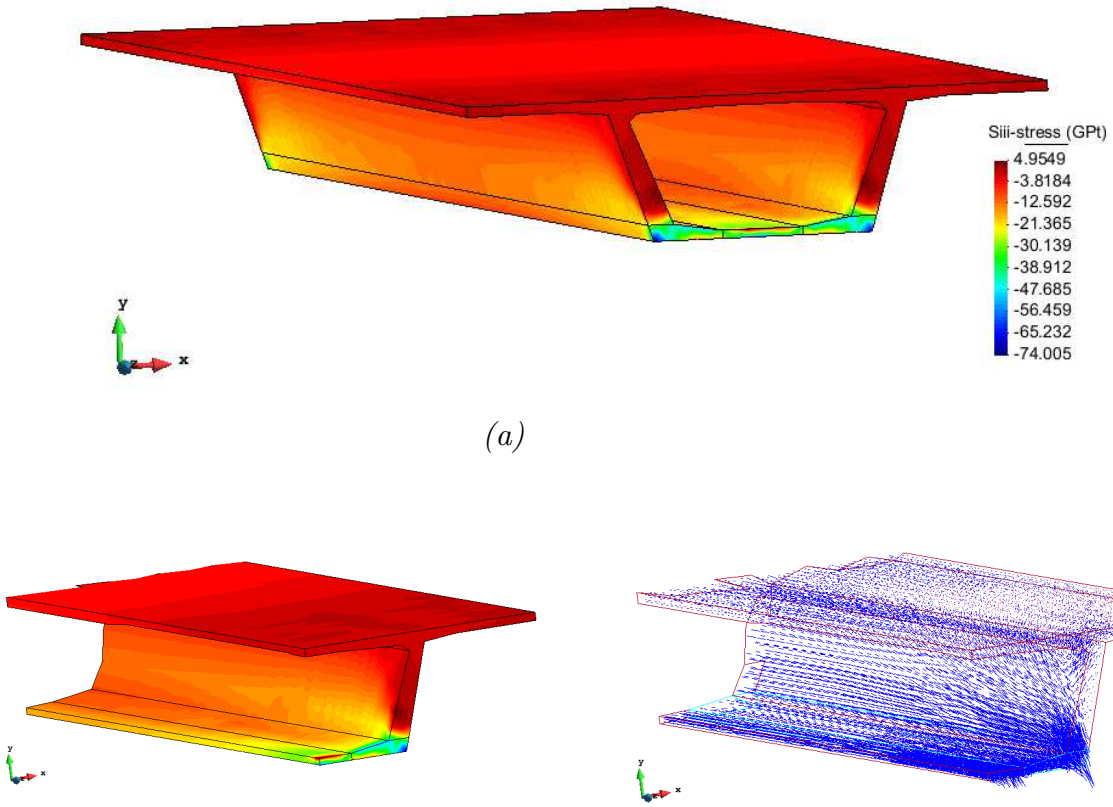

(a)

(b) *(c)*

Figure 5-10: Minimum principal stresses: (a) stress contours of full beam (MPa), (b) stress contours of cut beam portion (MPa), (c) stress vectors of cut beam portion

In Figure 5-9, region of high tensile stress can be seen at the end of the beam along its web and in the concrete region situated between the two anchorage prestressed area. This is more noticeable in Figure 5-9 (c) where stress vectors and the direction at which they are acting is shown. For instance, maximum tensile stress of 17 MPa was experienced in the web area while maximum tensile stress of 18 MPa was experienced in the middle region between the two anchorage areas. This phenomena can be explained by the spalling effect caused by the dispersion of prestress force in the anchorage zone. The values of tensile stresses are significantly high, and with such level of tensile stresses reached, the structure design is now governed by the ultimate limit state design, and hence need to be resized accordingly. Moreover, from Figure 5-10, it can be observed that there is a region of high compressive stresses in the anchorage area. For instance, a maximum compressive stress of 74 MPa was observed in the anchorage area. The values for the compressive stress in the anchorage area were significantly high, where it was found that it exceeds the maximum compressive strength of the concrete, which was set at 60 MPa. It is recommended to use higher strength concrete to avoid failure of the structure.

Now taking a look at the general distribution of stresses across the length of the box girder, it can be observed that region of high tensile stress occurs in the top fibre of the box girder. For instance, from Figure 5-9 and Figure 5-10, it was found that tensile stress of 0.6 MPa was experienced in the top fibre, while compressive stress of 8 MPa was experienced in the bottom fibre of the box girder at the middle span . This phenomenon can be explained by the hogging moment induced by the prestressing forces acting at an eccentricity to the centroid of the structure.

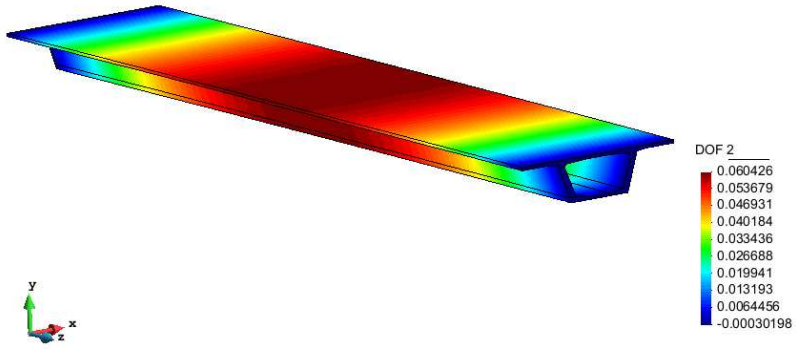

Figure 5-11: Displacement contours (m)

Figure 5-11 shows the displacement contours of the cambered beam. It can be seen that there is a general upward deflection of the beam, where the maximum deflection occurs at the middle span. For instance, the maximum deflection was found to be 60 mm upwards. It is believed that the upward deflection at middle span is due to the hogging moment caused by the prestressing force acting on the beam.

SLS stage

Figure 5-12 and Figure 5-13 respectively shows the maximum and minimum principal stresses of the box girder structure. Similar to the transfer stage, the colour code used in the figures is defined as follows: red colour represents region of maximum tensile stress while blue colour represents region of maximum compressive stress.

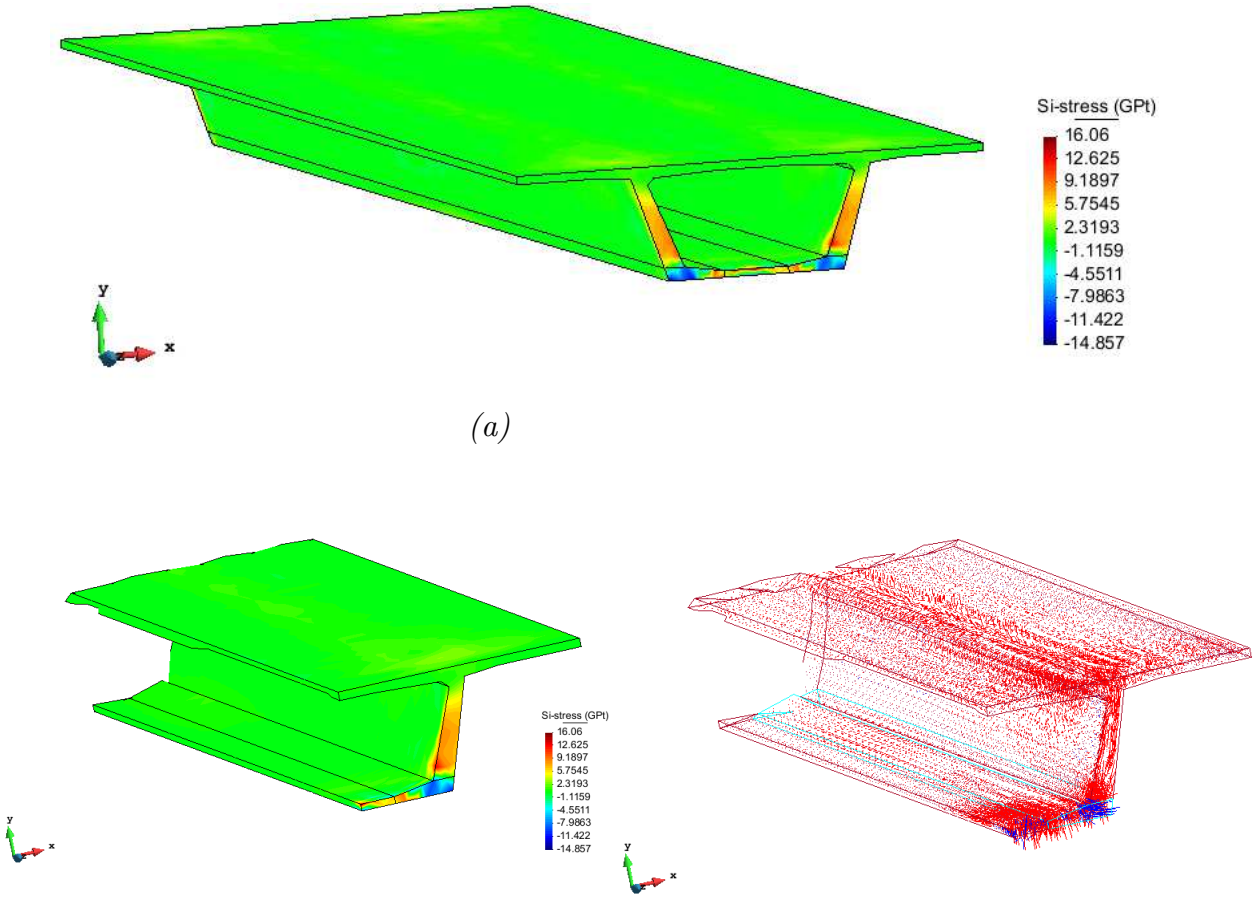

Figure 5-12: Maximum principal stresses: (a) stress contours of full beam (MPa), (b) stress contours of cut beam portion (MPa), (c) stress vectors of cut beam portion

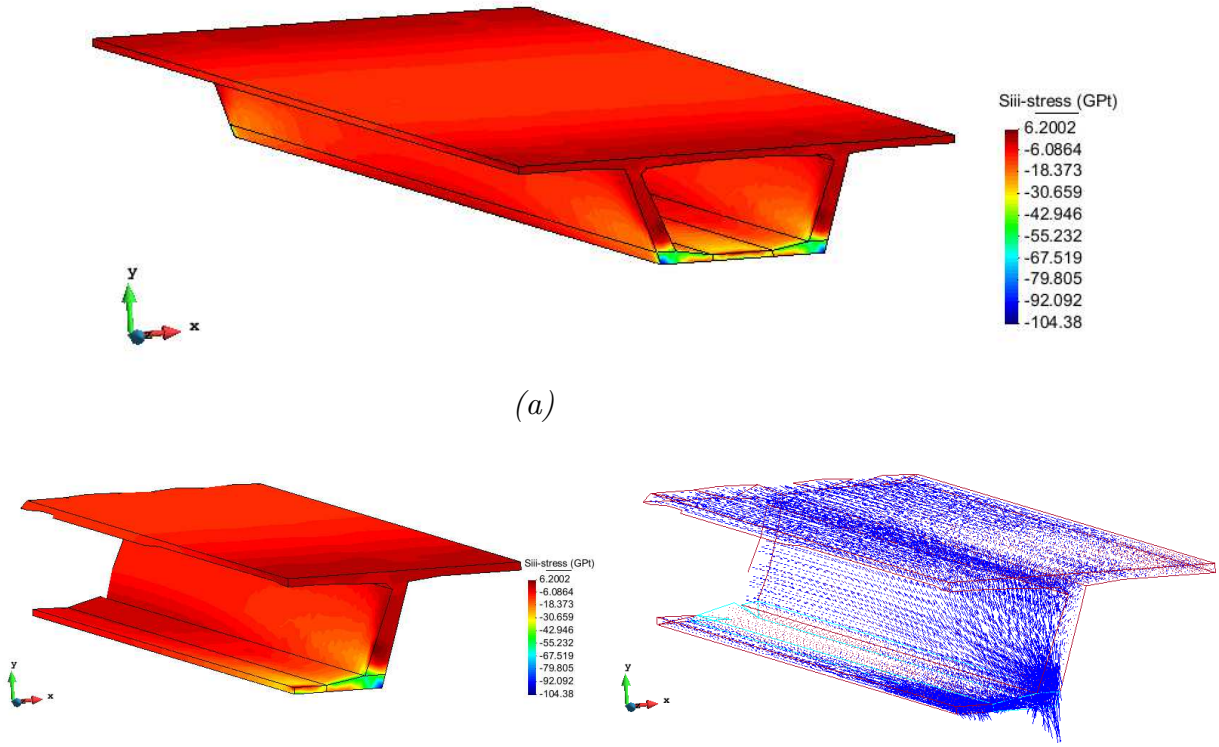

Figure 5-13: Minimum principal stresses: (a) stress contours of full beam (MPa), (b) stress contours of cut beam portion (MPa), (c) stress vectors of cut beam portion

Looking at the end faces section of the box girder in Figure 5-12 and Figure 5-13, the same kind of stress behaviour as in the transfer stage can be observed. That is, region of high tensile stress can be observed around the anchorage area. For instance, tensile stress of 7 MPa was observed in the web region while a tensile stress of 16 MPa was observed in the middle concrete region between the two anchorage areas. Moreover, compressive stress values of up to 104 MPa was observed in the anchorage area. This is a relatively high value, and exceed the compressive strength of the concrete by far. Using 100 MPa high strength concrete alone will not solve this failure issue, hence it is advised to distribute the prestressing forces over a larger area to avoid such high compressive stresses.

Now taking a look at the general distribution of stresses across the length of the box girder, although not noticeable on Figure 5-12 and Figure 5-13, it was found that region of high compressive stress occurs in the top fibre of the box girder while region of high tensile stress occurs bottom fibre of the box girder. For instance, the maximum compressive stress was found to be 0.6 MPa while the maximum tensile stress was found to be 2.4 MPa in the top and bottom fibre respectively. This behaviour suggest

that the sagging moment from the dead and live load had overcome the hogging moment from the prestress forces, hence it has a slight downward deflection at middle span. The following chapter gives more details on that matter.

5.3.5 Step 5: Checking final deformed shape

The deformed shape in SLS stage is shown in Figure 5-14.

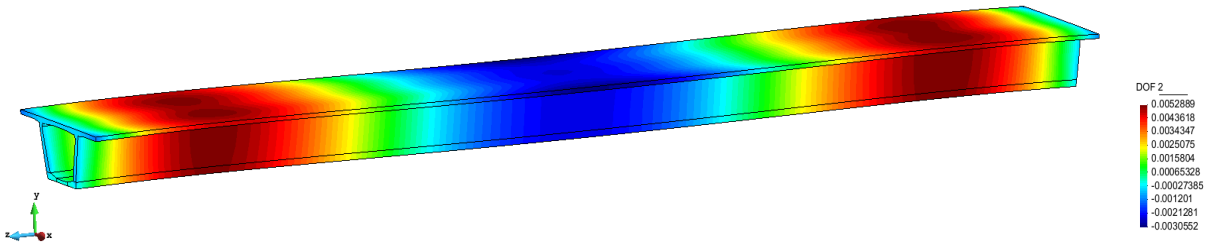

Figure 5-14: Displacement contours (m)

Figure 5-14 shows the displacement contours for the precast girder box in its final SLS stage using the forward analysis. It can be seen that at the middle span of the box girder, the structure has a downward deflection of 0.3 mm. It can also be seen that the structure has an upward deflection of 5 mm, characterized by the red colour region, in the areas adjacent to the middle span, then almost zero deflection at the support. This general behaviour is similar to the buckling effect of a structural member. Therefore, it can be concluded that the high prestressing force applied to the structure, acting in conjunction with live and dead load on the structure, is causing the buckling of the box girder. The buckling is however not noticeable considering the magnitude of the deflection and the size of the precast girder.

As discussed before, the inverse analysis method was used to obtain the required prestress forces to produce a desired final deformed straight member. The final known deformed state of the structure was taken as the starting point, and the analysis was performed backward until the required prestress force parameter was determined. Hence, now performing the forward analysis using the calculated prestress force, it should produce a structure that is close to the final known deformed state that was initially used in the inverse analysis. Hence to validate this theory, deflection at the middle span of Figure 5-14 was checked. The 0.3 mm deflection observed at the middle span was relatively small and can be said to be negligible for a structure of such size. This result, therefore, indicates that the use of the inverse analysis in achieving a desired final deformed state of the precast box girder portion of a bridge mega structure was successful.

6. Conclusion and recommendations

6.1 Conclusion

The aim of this study is to validate the method of inverse analysis in the computational analysis of prestressed concrete. Based on the results obtained in this study, a number of conclusions are drawn on different aspects covered.

6.1.1 Calibration of constitutive laws

In this study, the calibration of hypoelastic material in the modelling of the stress-strain behaviour of concrete was found to be successful. However, it was noted that the calibration was valid only up to the compressive strength of the concrete, and in the case of the study it was 60 MPa. Beyond that point, the power law of the hypoelastic material was found to no longer correlate to the experimental data.

Moreover, the calibration of Neo Hookean material was found to be unsuccessful for the purpose of this study. The stress-strain behaviour of the material law was found to follow a linear path, which couldn't fit the non-linear stress-strain behaviour of the experimental data. Therefore, it was concluded that, unless the computational analysis of concrete in this study is going to be based on a linear analysis, Neo Hookean material law cannot model concrete.

Lastly, linear hyperelastic material law was used to model for reinforcing bars and prestressing steel tendon. Owing to the simple linear stress-strain relationship in linear hyperelastic material, complex calibration was not required; the material parameters, to be used in the hyperelastic material law, were obtained from British Standards.

6.1.2 Material modelling

This study attempted to use an additive material type in the modelling of reinforced concrete. The results from the analysis were conclusive in using such material model, since the stress distribution in the concrete structure obtained from the computational simulations could be explained and backed up by the theory of principles of prestressed concrete developed in the literature review.

Similarly, the prestress body force implemented by Dr. Skatulla gave conclusive results; the prestress body force was reflecting accurately the behaviour of concrete under the action of prestress force placed at an eccentricity from the centroid of the structure.

6.1.3 Inverse analysis

Based on the results from section 4, it can be concluded that the use of inverse analysis was successful in predicting the final deformed shape of a prestressed I beam structure; which has a fairly simple geometry. Further use of the analysis method was done on a box girder precast units inspired from the Vasco da Gama Bridge. The structure was relatively massive with some level of complexities in its geometry, hence it was a relevant case study to test the capabilities of the inverse analysis. The results obtained were conclusive to the study.

6.2 Recommendations

Modelling and analysis of prestressed concrete structures is very complex. Recent researches have made significant breakthrough in the modelling of concrete and its composite where various physical mechanism within the concrete materials could be accounted for during analysis. Some of the factors are the effect of creep, shrinkage etc. This study did not take into account those mentioned factors due to the complexities involved in their modelling and the limited expertise of the author in the area of study. So a recommendation for future study in the field of concrete modelling would be to come up with a material law that will be able to model for the factors of creep, shrinkage and prestress losses in the material.

Moreover, further application of the inverse analysis can be investigated in the context of prestressed concrete analysis.

Lastly, the model of the prestress body force can be further improved by modelling for the individual tendons separately making it more realistic. Furthermore, a model of prestress losses can be proposed in future study to make the analysis more realistic.

7. References

Ahmad, S.H. & Shah, S.P. 1982. Complete triaxial stress-strain curves for concrete. *Journal of the Structural Division.* 108(4):728-742.

Ali, A.M., Farid, B. & Al-Janabi, A. 1990. Stress-Strain Relationship for concrete in compression made of local materials. *Engineering Sciences.* 2(1).

Barkanov, E. 2001. Introduction to the finite element method. *Institute of Materials and Structures Faculty of Civil Engineering Riga Technical University.*

Benaim, R. 2008. *The design of prestressed concrete bridges.* Taylor & Francis.

Bonet, J. & Wood, R.D. 1997. *Nonlinear continuum mechanics for finite element analysis.* Cambridge university press.

Burgoyne, C. 2005. Analysis of continuous prestressed concrete beams.

Buyukozturk, O. & Shareef, S.S. 1985. Constitutive modeling of concrete in finite element analysis. *Computers & Structures.* 21(3):581-610.

California Derpartment of Transportation, 2015. Available: http://www.dot.ca.gov/hq/esc/techpubs/manual/bridgemanuals/bridge-design-practice/bdp.html [2015, August 2015]

Chen, W. 2007. *Plasticity in reinforced concrete.* J. Ross Publishing.

Chen, W. & Duan, L. 2014. *Bridge Engineering Handbook: Construction and Maintenance.* CRC press.

Engel, J. & Kong, S.Y. Non-linear finite element analyses of prestressed concrete box-girder bridges subjected to shear and torsion.

Gerstle, K.H. 1981. Simple formulation of biaxial concrete behavior. *ACI Journal Proceedings.* ACI.

Gilbert, R.I. & Mickleborough, N.C. 1990. *Design of prestressed concrete.* CRC Press.

Grabow, M.J. 2004. Construction stage analysis of cable-stayed bridges. *Diplom Thesis.Civil and Environmental Engineering, Technical University of Hamburg Harburg, Germany.*

Hewson, N.R. 2003. *Prestressed concrete bridges: design and construction.* Thomas Telford.

Hewson, N. 2000. Design of prestressed concrete bridges. *The Manual of Bridge Engineering.* :241.

Hopkins, G., 2014. *Higly Non-linear Post-buckling Analysis of Shell Structures.,* Cape Town: University of Cape Town.

Houlsby, G.T. & Puzrin, A.M. 2007. *Principles of hyperplasticity: an approach to plasticity theory based on thermodynamic principles.* Springer Science & Business Media.

Hueste, M.B.D., Mander, J.B. & Parkar, A.S. 2012. *Continuous Prestressed Concrete Girder Bridges.Volume 1: Literature Review and Preliminary Designs.*

Instron, 2015. Compression Testing Concrete Cylinders. Available:http://www.instron.com.es/en/testing-solutions/by-material/concrete/compression/concrete-cylinders [2015, November 2015]

Kim, N. 2014. *Introduction to nonlinear finite element analysis.* Springer Science & Business Media.

Klinkel, S., Sansour, C. & Wagner, W. 2005. An anisotropic fibre-matrix material model at finite elastic-plastic strains. *Computational Mechanics.* 35(6):409-417.

Koshitawa. T., Ueda, M., Kikuchi, M. & Saito, T. Structural Performance of Precast Prestressed Concrete Frames with Hybrid Post-Tensioned Connections.

Lin, T.Y. & Burns, N.H. 1981. Design of prestressed concrete structures.

Lowes, L.N. 1999. *Finite Element Modeling of Reinforced Concrete Beam-Column Bridge Connections.*

Marshall, V. &. R. J., 1995. Prestressed concrete design and practice. *Concrete Society of Southern Africa, Prestressed Concrete Division*

Moradloo, J., Ahmadi, M.T. & Vahdani, S. Nonlinear Dynamic Analysis of Concrete Arch Dams.

Naaman, A.E., Naaman, A.E. & Naaman, A.E. 1982. *Prestressed concrete analysis and design: fundamentals.* McGraw-Hill New York.

Ogden, R.W. 1997. *Non-linear elastic deformations.* Courier Corporation.

Ottosen, N.S. & Ristinmaa, M. 2005. *The mechanics of constitutive modeling.* Elsevier.

PBWORKS, 2011. Available: http://id3124cl.pbworks.com/w/file/fetch/57897639/Vasco-Da_Gama_Bridge.pdf [2011, November 2015]

Rajagopal, V., Chung, J., Bullivant, D., Nielsen, P.M. & Nash, M.P. 2007. Determining the finite elasticity reference state from a loaded configuration. *International Journal for Numerical Methods in Engineering.* 72(12):1434-1451.

Raju, N.K. 2006. *Prestressed concrete.* Tata McGraw-Hill Education.

Ranzi, G. & Raymond , I. G., 2014. *Structural Analysis: Principles, Methods and Modelling.* New York: CRC Press.

Rao, S.S. 2005. *The finite element method in engineering.* Butterworth-heinemann.

Ratnayaka, D.D., Brandt, M.J. & Johnson, M. 2009. *Water Supply.* Butterworth-Heinemann.

Sack, K., 2014. *Biological tissue mechanics with fibres modelled as one dimensional Cosserat continua. Applications to cardiac tissue in healthy and diseased states.,* Cape Town: University of Cape Town.

Shuenn-Yih Chang, S. K. A. B. J. Z., 2012. *Advances in Civil Engineering and Building Materials.* Hong Kong: CRC Press.

Skatulla, S. & Sansour, C., 2015. On a path-following for non-linear solid mechanics with applications to structural and cardiac mechanics subject to arbitrary loading scenarios.

Tan, S., Yu, Z.W. & Zhang, H.S. 2012. Analysis and Computation Method of Prestressed Concrete Bridge in Construction Control. *Applied Mechanics and Materials.* Trans Tech Publ. 867.